nature communications

Article

https://doi.org/10.1038/s41467-025-57073-5

A rational multi-target combination strategy for synergistic improvement of non-ribosomal peptide production

Received: 24 September 2024

Accepted: 7 February 2025

Published online: 22 February 2025

Check for updates

Hao Yan[1,2,3], Zhenguo Xin[2], Ziwei Sang[1,2], Xingwang Li[1], Jia Xie[1], Jiale Wu[1], Shen Pang[2], Ying Wen[1] ✉ & Weishan Wang[2,3,4] ✉

Non-ribosomal peptides (NRPs) are pharmaceutically important natural products that include numerous clinical drugs. However, the biosynthesis of these NRPs is intricately regulated and improving production through manipulation of multiple regulatory targets remains largely empirical. We here develop a screening-based, multi-target rational combination strategy and demonstrate its effectiveness in enhancing the titers of three NRP drugs - daptomycin, thaxtomin A and surfactin. Initially, we devise a reliable colorimetric analog co-expression and co-biosynthesis reporter system for screening high-yielding phenotypes. Subsequently, through coupling CRISPR interference to induce genome-wide differential expression, we identify dozens of repressors that inhibit the biosynthesis of these NRPs. To address the challenge of multi-target combination, we further developed a dual-target screen approach and introduced an interplay map based on the synergy coefficient of each pairwise interaction. Employing this strategy, we engineer the final strains with multi-target synergistic combination and achieve the titer improvement of the three NRPs. Our work provides a rational multi-target combination strategy for production improvement of NRPs.

Microorganisms produce a diverse array of bioactive secondary metabolites (SMs), with non-ribosomal peptides (NRPs) representing a versatile class that includes antibiotics, immunosuppressants, anticancer agents, toxins, siderophores, pigments, and cytostatic[1,2]. *Streptomyces* species are renowned for contributing approximately two-thirds of these pharmaceutical molecules[3]. However, in wild-type (WT) *Streptomyces* strains, the production of NRPs is typically constrained due to the intricate and stringent regulatory networks, involving up to 12% of the total genome dedicated to regulatory genes[4,5]. This inherent regulation serves their own benefit rather than the objective of yield improvement in the pharmaceutical industry. Therefore, there is an urgent need to develop capabilities for identifying and reprogramming multiplexed synergetic regulators in order to redirect cellular resources towards NRP biosynthesis.

Construction of efficient microbial cell factories relies on globally tweaking the cell resources towards the biosynthesis of desired products, which is not always aligned with the direction of evolution that solely serves survival benefits[6,7]. Therefore, systematic engineering is required for harnessing multiplex regulatory targets to reprogram genome-wide metabolism. To achieve accurate engineering of multiple regulatory targets, two key challenges must be comprehensively addressed: firstly, the rapid identification of targets that can affect production performance; secondly, determining which targets can be synergistically combined to achieve greater improvement. Given the complexity of genetic interactions in biological systems, empirical

[1]State Key Laboratory of Animal Biotech Breeding and College of Biological Sciences, China Agricultural University, Beijing, China. [2]State Key Laboratory of Microbial Resources, Institute of Microbiology, Chinese Academy of Sciences, Beijing, China. [3]Beijing Key Laboratory of Genetic Element Biosourcing & Intelligent Design for Biomanufacturing, Beijing, China. [4]University of Chinese Academy of Sciences, Beijing, China. ✉e-mail: wen@cau.edu.cn; wangws@im.ac.cn

combinations of two or more regulatory targets do not always result in strains with improved performance[8,9]. Henceforth, it is imperative to develop an efficient rational strategy for combining synergistic multi-target in strain improvement.

Genome-scale identification of the engineering targets involves two interconnected steps: "mutation or interference" and "selection"[10,11]. Compared to existing methods for "mutation or interference"[12], such as CRISPR-based technology, which is a well-established and highly efficient mutation or interference tool used to identify functional target genes across various species[13,14], the strategy of "selection" presents greater challenges in identifying global targets[15]. For cases where desired products lack easily detectable characteristics such as color and growth-coupling traits, strain engineering often relies on available RNA-based riboswitches and transcription factor (TF)-based biosensors that respond to small molecules[16,17]. Nevertheless, the number of well-characterized riboswitches or TFs is still insufficient to meet the diverse sensing requirements for production purpose[15] – especially when it comes to detecting non-essential NRPs in *Streptomyces* species[18].

In addition to the lack of reliable and universal selection methods, a more pressing concern lies in the selection of targets that exhibit synergetic and additive effects for combinational engineering while discarding the antagonistic targets. This is because simultaneous mutation or interference of two genes usually produces a phenotype that is unexpected in light of each loss-of-function individual effect[19]. Therefore, investigating the underlying functional relationship between individual favorable targets and mapping these interactions would undoubtedly provide a rational guide of multi-target combinations, enabling highly efficient successive strain improvement[20]. However, we still face challenges in effectively combining individual favorable targets to generate synergistic effects in microbial strain improvement. Measurement of the synergy coefficient is a critical metric for evaluating the combined effects of multiple factors, such as in the synergistic screening of drugs[21], since this parameter quantifies how the interactions between the components either enhances or diminishes their individual effects. Therefore, the determination of synergistic coefficient should be introduced in the development of a rational multi-target combination strategy for synergistic improvement of non-ribosomal peptide producing strains.

To address the aforementioned challenges, we chose daptomycin natural producer *Streptomyces roseosporus*, thaxtomin A heterogeneous producer *Streptomyces coelicolor* and surfactin producer *Bacillus subtilis* as a proof-of-concept to develop strategies for identifying and combining multiplex synergistic targets. Daptomycin is recognized as a clinically significant antibiotic for treating of various bacterial infections[22]. Thaxtomin A is acknowledged as a natural herbicide approved by the U.S. Environmental Protection Agency with high selectivity for controlling common monocot and dicot weed in rice crops and turfgrass landscapes[23]. Surfactin is a cyclic lipopeptide, commonly used as an antibiotic for its capacity as a surfactant[24]. We initially develop an analog co-expression and co-biosynthesis reporter system to establish a correlation between daptomycin titer and colorimetric indigoidine level, and evaluate the feasibility of CRISPR interference (CRISPRi) systems in *S. roseosporus*. Subsequently, we target genome-wide regulatory genes in *S. roseosporus* using a CRISPRi library and identify a total of 17 targets that inhibit daptomycin biosynthesis. Furthermore, we devise a scalable CRISPRi-based dual-screen strategy enabling massively parallel pairwise inhibition of these identified targets. By calculating synergy coefficient q of the pairwise combinations, we map the relationships between these targets and simultaneously engineer four targets with synergistic effect for high-yield construction. The resulting strain achieves a titer of 1054 mg/L in a 7.5-L fermenter, which, to the best of our knowledge, surpasses the previous highest reported yields in fermenters (812 μg/mL)[25]. Furthermore, we demonstrate the broad applicability of this multi-target rational combination strategy by improving thaxtomins A titer to 352 mg/L in heterologous host *S. coelicolor* 1152 and surfactin titer to 878 mg/L in *B. subtilis*. Previously, the yield of thaxtomin A was increased to 728 mg/L and 504.6 mg/L in *Streptomyces albidoflavus* J1074[23] and *Streptomyces coelicolor* M1154[26], respectively, through combinatorial metabolic engineering and promoter engineering. To our knowledge, this work represents the first application of rational strategy for combining multiple targets in strain engineering.

Results

Overview of the screening-based rational multi-target combination strategy

The naturally occurring cellular regulation and metabolism networks were evolved to adapt to diverse environmental conditions for the survival benefit. Therefore, it is imperative to reconfigure this intricate network with the aim of achieving optimal production. In the past decade, numerous target screening strategies have been developed to identify independent regulatory targets that can enhance production[27]. However, there is currently a lack of reliable theory or data-driven guidance on how to effectively combine these targets to achieve synergistic improvement. The existing trial-and-error combination strategy primarily relies on empirical combinations, which often result in inferior outcomes compared to single-target operations (Fig. 1 with gray background).

Compared to other microbial products, the biosynthesis of SMs in *Streptomyces* is subject to more intricate regulation[28,29]. This necessitates the identification of genome-scale regulatory targets to inform combinational engineering of these multiple targets for synergistic performance. To achieve this objective, we developed a transferable screening-based rational multi-target combination strategy (Fig. 1 with light blue background). Following the individual target screening, we further established a method for screening the pairwise combinations of these targets. Subsequently, by determining the relationship between these targets and integrating their interactions into a network, we were able to identify multiple targets with positive synergistic effects. Finally, these synergistic targets were applied in strain improvement to achieve rational multi-target engineering.

Construction of an analog co-expression and co-biosynthesis reporter system

Initially, we established a universal reporter system that offers convenience and reliable indication of high-yield phenotypes for desired NRPs. We chose daptomycin produced by *S. roseosporus* as a proof-of-concept for developing this universal reporter system. Similar to other NRPs, daptomycin undergoes a complex and multifaceted regulatory process[30] that coordinates the initiation of daptomycin biosynthesis and its related physiological events, including expression of the daptomycin biosynthetic gene cluster (BGC), provision of cofactors and precursors, maintenance of production morphology, and other relevant pathways (Fig. 2a). These multiplex targets constitute a functional group that collectively orchestrate daptomycin biosynthesis. We therefore devised an analog co-expression and co-biosynthesis reporter system to accurately reflect the efficiency of the representative daptomycin biosynthetic machinery within this group. Specifically, we chose another NRP type indigoidine BGC containing only a single module NRP synthase (NRPS) gene (*idgS*) and a 4′-phosphopantetheinyl transferase (*sfp)* from *Streptomyces lavendulae* to be co-expressed with daptomycin BGC by inserting the promoterless *idgS-sfp* into the 3′ end of *dptD* (Fig. 2a and Supplementary Fig. 1a). Since both products - daptomycin and indigoidine - belong to NRPs, measuring colorimetric indigoidine levels can not only reflect the expression level of the daptomycin BGC and its related genes but also indicate other common targets that contribute to NRP biosynthesis. Therefore, our developed reporter system featuring analog

https://doi.org/10.1038/s41467-025-57073-5

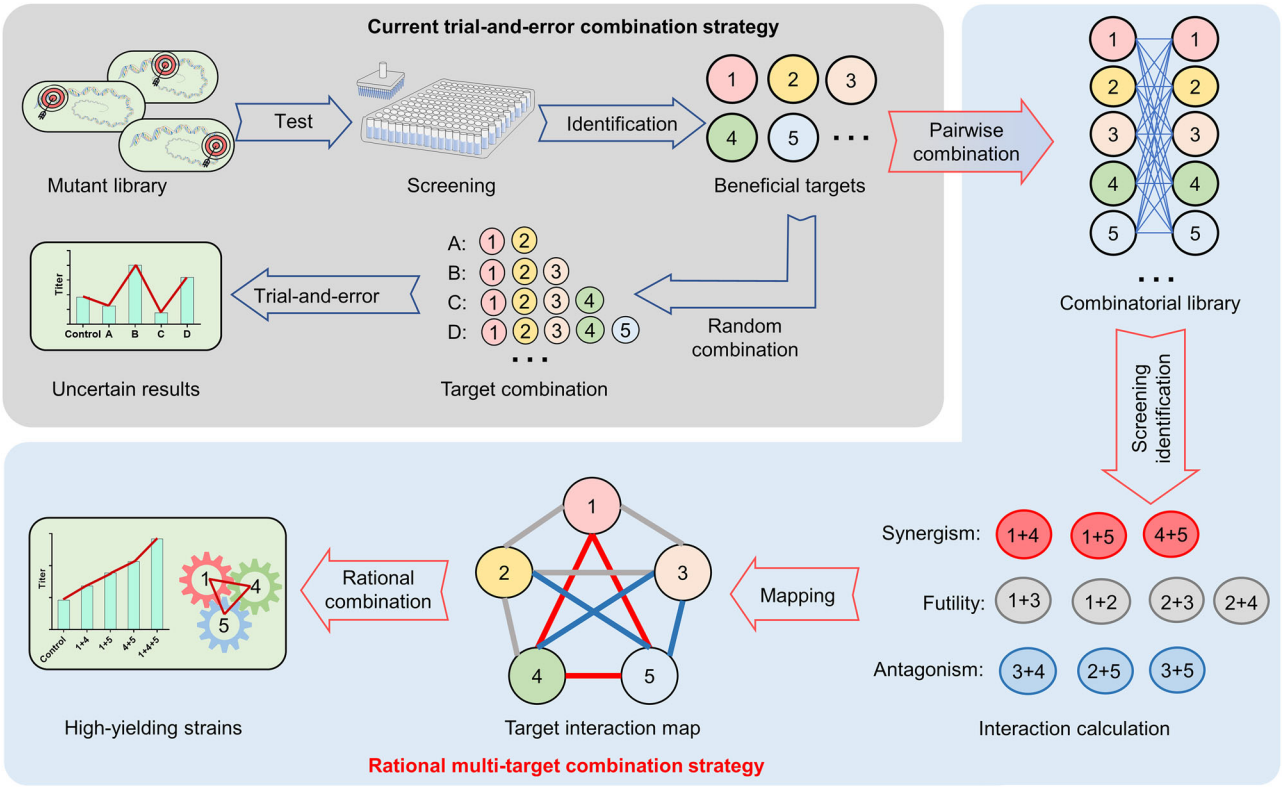

Fig. 1 | Overview of the screening-based rational multi-target combination strategy. The traditional trial-and-error approach for random target combination is depicted with gray background, while our screening-based rational multi-target combination strategy is distinguished by blue background.

co-expression and co-biosynthesis could improve the reliability in reporting the NRP high-yield phenotype.

To assess the availability of *idgS-sfp* in *S. roseosporus*, *idgS-sfp* under control of the *dptEp* or *ermE*p* promoters was integrated into WT chromosome, respectively. We observed both resulting strains exhibited blue pigment on DA1 plates or in liquid medium (Supplementary Fig. 1b, c), indicating successful expression of indigoidine. Spectral scanning revealed a maximum absorption peak at 600 nm for indigoidine (Supplementary Fig. 1d), with its level being linearly and positively correlated with OD_{600} value (Supplementary Fig. 1e), demonstrating the convenient use of indigoidine as a reporter for colorimetric end-point assays. We next inserted the *idgS-sfp* cassette after the stop codon of *dptD* by homologous recombination to construct the analog co-expression and co-biosynthesis reporter strain Srdi (Supplementary Fig. 2a–c). Reverse transcription PCR analysis revealed a large polycistronic transcript encompassing *dptEFABCD-idgs-sfp-dptGH* (Supplementary Fig. 2d), indicating this strategic placement of *idgS-sfp* within the daptomycin BGC ensured coordinated expression and biosynthesis of both daptomycin and indigoidine compounds. Subsequently, we assessed the impact of *idgS-sfp* on cell growth and daptomycin production. We did not observe significant difference in cell growth and daptomycin production between WT and Srdi fermentation broth samples (Supplementary Fig. 2e–f).

To evaluate the correlation between indigoidine production and daptomycin titer, we employed two strategies to perturb daptomycin titers in Srdi. Firstly, we individually overexpressed two activators (AtrA, BldD)[30,31] and two repressors (DasR, WblA)[32,33] known to influence daptomycin production in Srdi. Secondly, we replaced the native promoter of *dptEFABCD-idgs-sfp-dptGH* operon with a strong promoter *kasO*p*. Our finding revealed a positive correlation between indigoidine production and their respective daptomycin titer in overexpression strains $Srdi^{OatrA}$, $Srdi^{ObldD}$, $Srdi^{OdasR}$, $Srdi^{OwblA}$, $Srdi^{kasOdpt}$ and control strain $Srdi^{1139}$ ($R^2 = 0.95662$) (Fig. 2b), indicating the colored NRP indigoidine faithfully reported the level of co-expressed and co-biosynthesized daptomycin. Additionally, we also observed a positive correlation between the transcript level of the *dptEFABCD-idgs-sfp-dptGH* operon and the corresponding daptomycin titer ($R^2 = 0.86465$) (Fig. 2c), suggesting the expression level of daptomycin BGC could serve as an indicator for daptomycin biosynthesis to some extent. However, the indigoidine level showed a weaker correlation with the transcript abundance of daptomycin BGC compared to that with the titer of daptomycin (Fig. 2b and Supplementary Fig. 2g), suggesting that apart from genes contributing to co-transcription, other targets beneficial for NRP biosynthesis also played a noticeable role. These results indicated that our designed NRP analog co-expression and co-biosynthesis reporter system could accurately detect and quantify changes in daptomycin titer.

An exception further demonstrated the advantage of our reporter system. We observed a higher expression level of *dptEFABCD-idgs-sfp-dptGH* operon in $Srdi^{kasOdpt}$ compared to that in $Srdi^{ObldD}$; however, both daptomycin and indigoidine yields were lower (Fig. 2d and Supplementary Fig. 2g). This discrepancy arises from the fact that $Srdi^{kasOdpt}$ solely enhances daptomycin production through upregulating the expression of daptomycin BGC, while $Srdi^{ObldD}$ involves coordinated regulation of a group of related genes responsible for daptomycin biosynthesis. This hypothesis was validated through comparative transcriptome analysis of these strains: only a significant upregulation in the expression levels of daptomycin BGC was observed in $Srdi^{kasOdpt}$ (Fig. 2e); in contrast, multiple alterations were found in the expression levels of genes involved in amino acid metabolism, cofactor metabolism, morphology, and other related processes besides the daptomycin BGC in $Srdi^{ObldD}$ (Fig. 2f). Similarly, this pleiotropic perturbation was also observed in $Srdi^{OatrA}$ (Fig. 2g). Based on this finding, we concluded that our developed NRP analog co-expression and co-biosynthesis reporter system was qualified for identifying targets with pleiotropic effects on daptomycin production.

https://doi.org/10.1038/s41467-025-57073-5

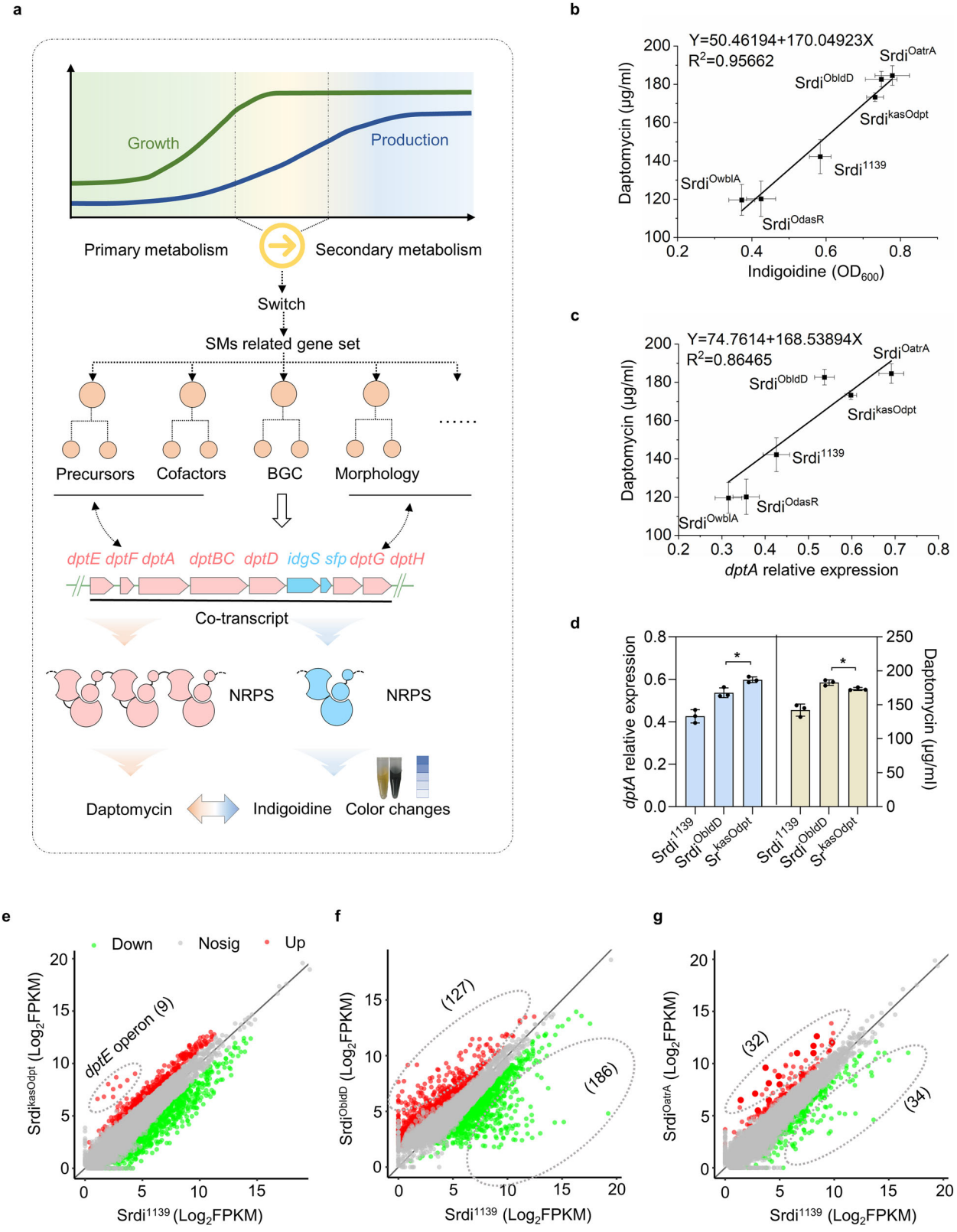

Evaluation of CRISPRi using the developed reporter system

Having developed a reliable reporter system, we proceeded to evaluate the availability of the established CRISPRi system in other *Streptomyces* species[34] for target screening in *S. roseosporus*. We selected *bldD*, encodes a global transcription factor, as target due to its role in activating daptomycin production and repressing morphological differentiation[30]. Following the rule that single guide RNA (sgRNA) targeting the non-template strand (NT) are highly effective[34], we designed a sgRNA specifically targeting *bldD*. Our result revealed that inhibition of *bldD* (strain WT^{bldDi}) led to a phenotype similar to that of a *bldD* deletion mutant ΔbldD[30], displaying earlier and enhanced sporulation on DA1 plate (Fig. 3a). Further transcript analysis of *bldD* indicated a 54% reduction in WT^{bldDi} strain compared to WT and WT^{-} (containing plasmid without sgRNA) (Fig. 3b). Inhibition of *bldD*

Fig. 2 | Design and characterization of the reporter system. a Schematic diagram of reporter system. The promoterless reporter genes *idgS-sfp* are fused downstream of *dptD*, resulting in an overlap between the TGA stop codon of *dptD* and the ATG start codon of *idgS*. The co-transcription of the *dptEFABCDGH* operon is indicated by a solid black underline. **b** Correlation between daptomycin titer and indigoidine level in Srdi derivatives expressing known targets, namely Srdi^{OatrA}, Srdi^{ObldD}, Srdi^{OdasR}, and Srdi^{OwblA} (corresponding to *atrA*, *bldD*, *dasR*, and *wblA* overexpression in Srdi). Control strains Srdi^{1139} contains empty plasmid pKC1139 and Srdi^{kasOdpt} was replaced by the native promoter *dptEp* with the strong promoter *kasO*p* in Srdi. **c** Correlation between daptomycin titer and daptomycin BGC expression level in Srdi derivatives. Here we used the transcript of *dptA* as a representative measure for the expression of the daptomycin BGC. **d** Daptomycin titer and daptomycin BGC expression level in Srdi^{1139}, Srdi^{ObldD}, and Srdi^{kasOdpt}. Two-tailed Student's *t* test [$^{*}p < 0.05$. $p = 0.016634191$, 0.025531917 (left to right)]. **e** Comparative transcriptomic analysis of Srdi^{kasOdpt} and Srdi^{1139}. Genes with significantly differential expression levels are circled with gray dot line. The numbers in parentheses represent the count of genes displaying significant differential expression levels. **f** Comparative transcriptomic analysis of Srdi^{ObldD} and Srdi^{1139}. **g** Comparative transcriptomic analysis of Srdi^{OatrA} and Srdi^{1139}. Data in (**b**, **c**, **d**) are shown as the mean ± SD ($n = 3$ biological replicates).

transcription resulted in lower expression levels of daptomycin BGC in WT^{bldDi} strain compared to WT, while higher than ΔbldD (Fig. 3b). Consistent with these findings, daptomycin titer exhibited the same trends (Fig. 3c). Collectively, these results demonstrated that the CRISPRi system could be employed for construction of CRISPRi library in *S. roseosporus*.

To test the applicability of CRISPRi with our developed analog co-expression and co-biosynthesis reporter system, we firstly conducted a mock test using known repressor *wblA*[33] of daptomycin biosynthesis (Fig. 3d). We generated Srdi^{wblAi} strain with CRISPRi targeting *wblA* in Srdi. In comparison to parent Srdi and control strain Srdi^{-} (containing plasmid without sgRNA), the color intensity of this strain noticeably deepened in three-day culture (Fig. 3e and Supplementary Fig. 3a). The transcription level of *wblA* was decreased by 70%, while that of daptomycin BGC increased by 2- to 3-fold in Srdi^{wblAi} compared to that in Srdi^{-} (Supplementary Fig. 3b). Consequently, we observed a corresponding increase of around 30% in daptomycin titer in Srdi^{wblAi} (Fig. 3f), similar to the inhibition of *wblA* in WT using the same approach (a 26% increase, Fig. 3f). These results indicated that integration of the CRISPRi library with the analog co-expression and co-biosynthesis reporter system enables identification of targets influencing daptomycin production.

To further evaluate the compatibility of our analog co-expression and co-biosynthesis reporter system with the CRISPRi library for identifying unknown targets, we performed a mini-library screening using a CRISPRi approach. Specifically, we chose 11 TetR-family TFs (*tetR1* through *tetR11*) located upstream or downstream of transporter as potential targets (Supplementary Fig. 3c). Subsequently, we constructed the library comprising sgRNA targeting the 11 *tetR* genes and known repressor *wblA*, which was then transformed into reporter strain Srdi (Fig. 3d). We randomly selected 100 transformants to measure indigoidine level with microplate reader and evaluate the bias towards targeted genes in these samples. Remarkably, all 13 genotype strains including the control strain Srdi^{-} were presented among the selected transformants (Fig. 3g). Furthermore, we determined the daptomycin titer for each strain and observed a strong linear relationship with the indigoidine level ($R^2 = 0.90743$) (Fig. 3h). These findings confirmed that our reporter system and CRISPRi library are highly compatible for efficient identification of unknown targets influencing daptomycin production.

We observed a noticeable darkening in the blue color of Srdi^{tetR6i} and Srdi^{tetR7i} (Fig. 3g and Supplementary Fig. 3d), indicating *tetR6* and *tetR7* function as negative regulators for daptomycin production. Subsequently, our transcription assay revealed a substantial increase in the transcripts of both daptomycin BGC and *idgS* in Srdi^{tetR6i} and Srdi^{tetR7i} compared to that in Srdi^{-} (Fig. 3i). Furthermore, we validated the inhibitory effect of *tetR6* and *tetR7* on daptomycin titer by individually deleting these genes in the WT strain (Supplementary Fig. 3e, f). Deletion mutants ΔtetR6 and ΔtetR7 exhibited an increase daptomycin titer by 35% and17% compared to WT, respectively (Fig. 3j), which correlated with enhanced indigoidine level (Fig. 3g). Taken together, these results suggested that combining CRISPRi library with the analog co-expression and co-biosynthesis reporter system could be utilized for identifying targets that inhibit daptomycin biosynthesis.

Screening targets inhibiting daptomycin production

Aiming to identify targets that directly or indirectly inhibit daptomycin production, we designed a pool of sgRNAs targeting all 610 predicted regulator genes in *S. roseosporus* genome, with three sgRNAs targeting different sites of each gene on the NT strand. The schematic representation of our screening workflow is depicted in Fig. 4a. Briefly, a plasmid library harboring 1830 unique sgRNA was transformed into reporter strain Srdi, and transformants exhibiting darker blue color on RM14 plates were selected for further screening through indigoidine quantitation in microplates. Transformants showing higher indigoidine level compared to Srdi were subjected to sequencing for identification of the targeted genes.

The coverage of sgRNAs in both the CRISPRi plasmid library and Srdi transformants were determined using next generation sequencing (NGS). In the plasmid library, all 610 regulatory genes were targetable, with up to 87.4% of genes having three sgRNAs available for targeting and the total sgRNA coverage was 95.2% (Fig. 4b). Among Srdi transformants, the total sgRNA coverage was 81.6% where more than half of the genes (58.0%) were targeted with three sgRNAs and only one gene (0.2%) remained untargeted (Fig. 4c). Subsequently, over 300 darker blue colonies were visually screened from a pool of more than 20,000 transformants. (Supplementary Fig. 4a). These colonies were further subjected to an indigoidine colorimetric assay for quantification purposes (Fig. 4d and Supplementary Fig. 4b), leading to the discovery of 16 regulators that inhibit daptomycin synthesis (their genes were named as *idt1* through *idt16*, Supplementary Fig. 4b). These regulators included one SARP-family, one LysR-family, one LacI-family, three MarR-familiy, four TetR-familiy, one XBE-family, one IclR-family, one Crp/Fnr-family, one MerR-family, one GntR-family, and one WhiB-family regulators. Transformants inhibiting these targets by cognate sgRNA exhibited a significant increase in daptomycin titer ranging from 17.4% to 37.8% compared to control strain Srdi^{-} (Fig. 4d). Notably, *wblA* and *tetR6*, which had been previously identified as a repressor for daptomycin production, were also included among the 16 screened genes, suggesting the reliability of our screening workflow.

We ranked these 16 targets based on their indigoidine output, which was consistent with the measurement of daptomycin production (Supplementary Table 1). To validate the identified targets, we randomly selected targets *idt4*, *idt5*, *idt6*, and *idt7* to construct cognate mutant strains Sr4-Q57*, Sr5-Q22*, Sr6-Q94*, and Sr7-Q6*, respectively (Supplementary Fig. 4c). Shake-flask fermentation and qRT-PCR analyses revealed that loss-of-function of the four genes all led to an elevated daptomycin titer (Fig. 4e), as well as an increased expression of daptomycin BGC compared to WT (Fig. 4f). These results confirmed the inhibitory role of our identified targets in daptomycin production.

To further enhance daptomycin titer, we performed combinational inactivation by targeting two out of the four confirmed targets (*idt4*, *idt5*, *idt6*, and *idt7*) in WT, generating mutant strains Sr45, Sr46, Sr47, Sr56, Sr57, and Sr67. Surprisingly, we observed that daptomycin titer of Sr46 was lower than that of WT, and that the titer of Sr47 and Sr57 had no obvious change (Fig. 4g). These findings suggested that random combinations of these targets did not yield synergetic effects on enhancing daptomycin titer. Therefore, gaining insights into the

https://doi.org/10.1038/s41467-025-57073-5

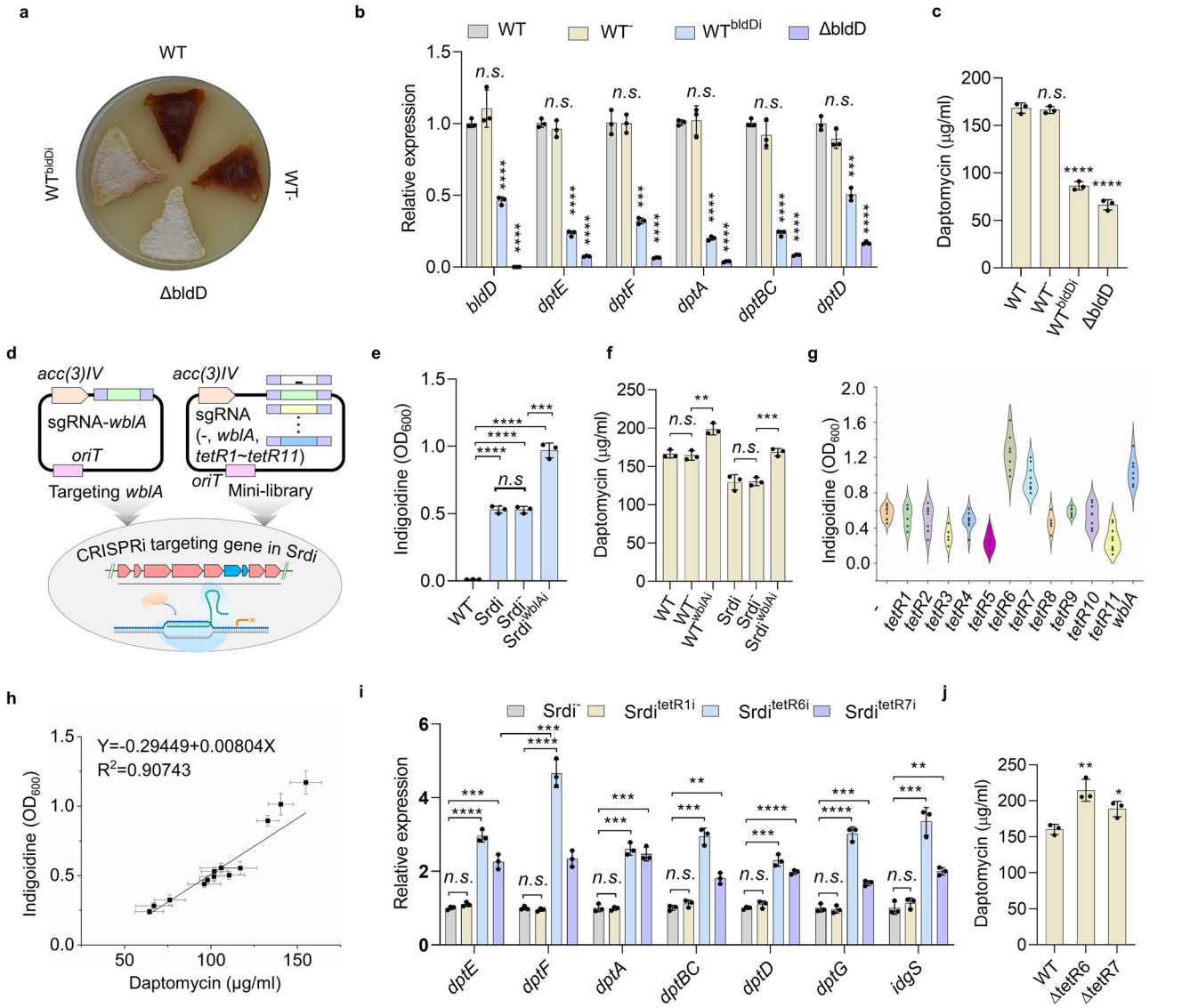

Fig. 3 | Test of CRISPRi-based reporter system for screening in *S. roseosporus*. **a** Phenotypes of WT, ΔbldD (*bldD* deletion mutant), WT^{bldDi} (*bldD*-inhibited mutant), and the control strain WT^{-} (WT with pSETdCas9Rg-2). These strains were grown on DA1 plates at 28 °C for 5 days. **b** Transcription levels of *bldD* and genes of daptomycin BGC in WT, WT^{-}, WT^{bldDi}, and ΔbldD. Samples were collected after 6 days growth on DA1 plate. [p = 0.253602325, 1.99842E−05, 5.07332E−07, 0.338845868, 2.80015E−06, 7.24141E−07, 0.926512747, 0.00016914, 4.31204E−05, 0.818549401, 4.86554E−07, 1.11713E−07, 0.218100115, 2.23403E−06, 5.25857E−07, 0.085602875, 0.00021213, 9.19636E−06 (left to right)]. **c** Daptomycin titer of WT, WT^{-}, WT^{bldDi}, and ΔbldD grown in fermentation medium for 10 days. [p = 0.621013707, 3.34048E−05, 2.02346E−05 (left to right)]. **d** Schematic for evaluating the compatibility between CRISPRi and our developed reporter system through introducing a single target or mini-librariy. **e** Indigoidine level in WT^{-}, Srdi, Srdi^{-} (Srdi with plasmid pSETdCas9Rg-2), and Srdi^{wblAi} (Srdi with inhibited *wblA*). [p = 4.46815E−06, 3.68173E−06, 7.32406E−06, 0.988813111, 0.000230028 (left to right)]. **f** Daptomycin titer in WT, WT^{-}, WT^{wblAi}, Srdi, Srdi^{-}, and Srdi^{wblAi} grown in fermentation medium for 10 days. [p = 0.703966652, 0.00359405, 0.906149569, 0.000788765 (left to right)]. **g** Indigoidine levels of transformants with the mini-library. Specifically, "−" denotes the control strain Srdi^{-}; *tetR1* through *tetR11* represents strains with CRISPRi-inhibited *tetR1* through *tetR11*, respectively; *wblA* indicates Srdi^{wblAi}. Here the indigoidine levels of 100 transformants covering all the 11 targets were determined and showed in the violin plots. **h** Correlation between daptomycin titer and indigoidine level in Srdi derivatives Srdi^{-}, Srdi^{tetR1i} through Srdi^{tetR11i}, and Srdi^{wblAi}. **i** Transcription levels of daptomycin BGC genes and *idgS* in Srdi^{-}, Srdi^{tetR1i}, Srdi^{tetR6i}, and Srdi^{tetR7i} grown in seed medium for 2 days. [p = 0.078571011, 3.84465E−05, 0.000447016, 0.271714823, 7.81638E−05, 0.00051151, 0.814630767, 0.000153486, 0.000297848, 0.158558972, 0.000137847, 0.001065091, 0.195323921, 0.000152317, 1.79512E−05, 0.682506353, 9.25055E−05, 0.000782728, 0.377330586, 0.000588997, 0.001023336 (left to right)]. **j** Daptomycin titer of WT, ΔtetR6 (*tetR6* deletion mutant), and ΔtetR7 (*tetR7* deletion mutant). [p = 0.005056642, 0.019752034 (left to right)]. Data in (**b**, **c**, **e**, **f**, **h**, **i**, **j**) are shown as the mean ± SD (n = 3 biological replicates). Two-tailed Student's t test was used in (**b**, **c**, **e**, **f**, **i**, **j**) to analyze the statistical significance (*n.s.*, not significant (p > 0.05); *p < 0.05; **p < 0.01; ***p < 0.001; ****p < 0.0001).

cooperative interactions among the identified targets is crucial for further titer improvement.

Development of a dual-target screening approach

To identify the cooperative targets, we developed a construct that enables simultaneous dual-target inhibition by CRISPRi to conduct synergistic screening with the analog co-expression and co-biosynthesis reporter system (Fig. 5a). Specifically, we designed a synergistic library targeting pair of genes simultaneously to assess their effects on reporter output. Initially, we evaluated the efficiency of simultaneous dual-target inhibition through CRISPRi by targeting *gfp* and *mCherry* in *S. roseosporus*. Laser confocal microscopy observation (Fig. 5b) and fluorescence quantification assays (Fig. 5c) demonstrated effective parallel inhibition (>70%) of both *gfp* and *mCherry* by

https://doi.org/10.1038/s41467-025-57073-5

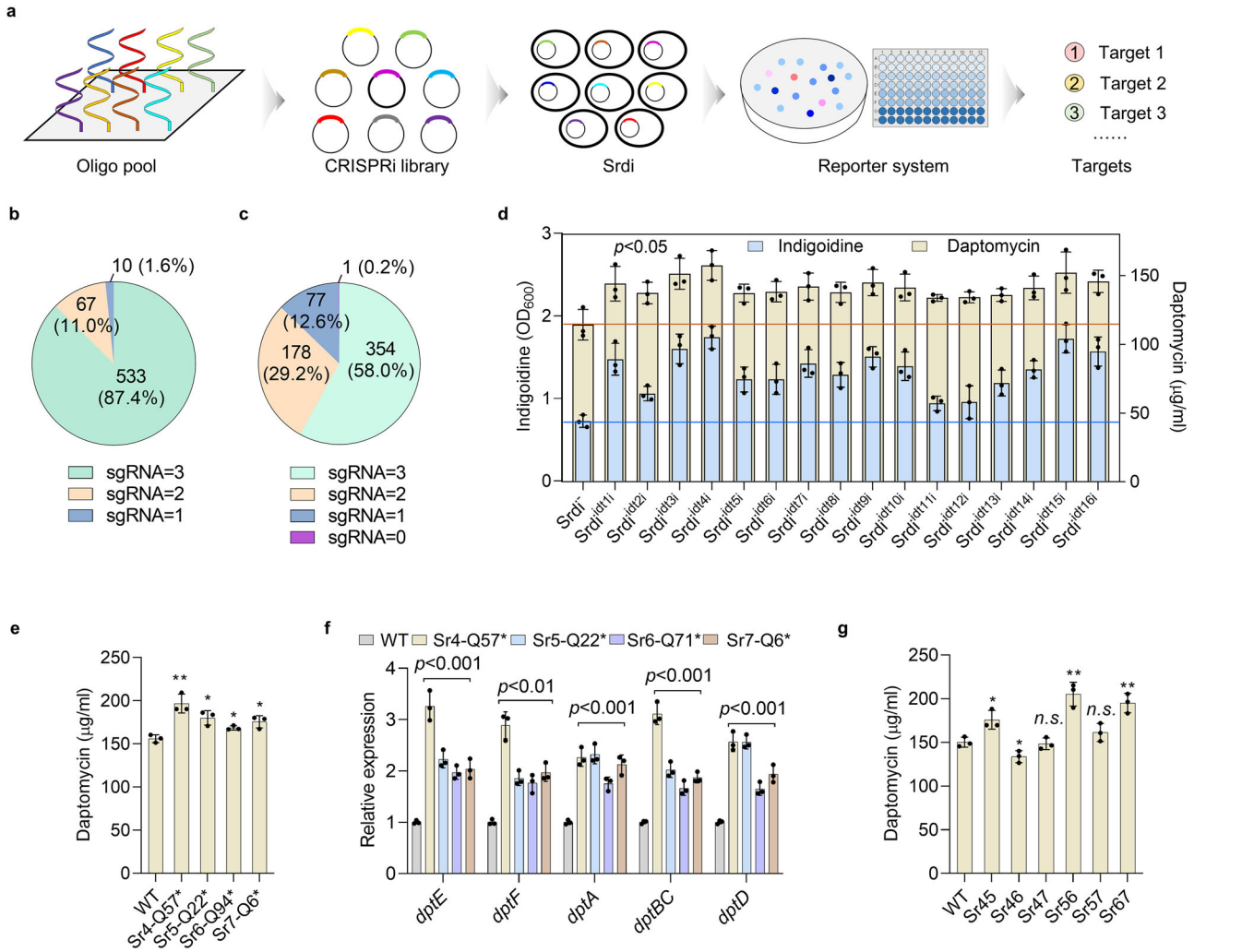

Fig. 4 | Screening targets that inhibit daptomycin production. a Workflow for screening targets that inhibit daptomycin production. **b** Coverage of sgRNAs in CRISPRi plasmid library. **c** Coverage of sgRNAs in Srdi transformants. Since three target sites were designed for each gene, "sgRNA=3" means that all three target sites were detected. Similarly, "sgRNA=2", "sgRNA=1", and "sgRNA=0" mean that only 2, 1, and 0 of the three target sites were detected, respectively. **d** Indigoidine level and daptomycin titer when inhibiting the identified targets in Srdi. The blue and brown lines indicate the indigoidine levels and daptomycin in the control strain Srdi-, respectively. [p = 0.003282553, 0.007464338, 0.001446173, 0.00034476, 0.006491144, 0.010929629, 0.002683903, 0.0044472, 0.000722168, 0.00359535, 0.031076087, 0.13338661, 0.009880467, 0.001124236, 0.000753792, 0.00158046 (indigoidine: left to right); p = 0.036945733, 0.0432256, 0.015491013, 0.008536545, 0.03695489, 0.036148854, 0.032078525, 0.037558817, 0.022461226, 0.034004881, 0.041198351, 0.043306871, 0.035889288, 0.030190684, 0.024581079, 0.016597474 (daptomycin: left to right)]. **e** Daptomycin titers of WT and double mutant strains Sr4-Q57*, Sr5-Q22*, Sr6-Q71*, Sr7-Q6*. [p = 0.004047725, 0.011340892, 0.013594525, 0.015901674 (left to right)]. **f** Transcription levels of daptomycin BGC in WT, Sr4-Q57*, Sr5-Q22*, Sr6-Q71*, and Sr7-Q6*. Samples were collected after 2 days culture in seed medium. [p = 0.000182357, 0.000231765, 0.000228029, 0.000764954, 0.000249225, 0.000577618, 0.002118873, 0.000747447, 0.000276501, 0.000261965, 0.000660066, 0.000529196, 6.63681E−05, 0.000301623, 0.001158026, 0.000150468, 0.000139481, 3.71049E−05, 0.000910931, 0.000764598 (left to right)]. **g** Daptomycin titer in WT and double mutant strains Sr45, Sr46, Sr47, Sr56, Sr57, Sr67. [p = 0.021964853, 0.03252863, 0.739909874, 0.003015842, 0.182164021, 0.003489912 (left to right)]. Data in **d**–**g** are shown as the mean ± SD (n = 3 biological replicates). Two-tailed Student's t test was used in **d**–**g** to analyze the statistical significance (*n.s.*, not significant ($p > 0.05$); *$p < 0.05$; **$p < 0.01$; ***$p < 0.001$).

CRISPRi. Subsequently, we constructed a pairwise combinatorial library comprising the 17 identified target genes, and ensured coverage of all the combinations through NGS confirmation.

After transforming the pairwise combinatorial library into reporter strain Srdi, we randomly sequenced 600 colonies to quantify the synergistic effects of all the 171 combinations. Once again, we observed that the random combination of two favorable targets generated a great deal of uncertainty and does not always result in improved production performance (Fig. 5d). Subsequently, we chose five combinations with high levels (SrdiC1 through SrdiC5) and five combinations with low levels (SrdiC6 through SrdiC10) to measure daptomycin titer. As expected, their titers exhibited a consistent trend with their corresponding indigoidine level (Fig. 5e, f). These results underscored that our strategy of simultaneous dual-target screening provided a reliable guide for engineering two target combinations (Fig. 5e, f).

Synergistic multi-target engineering

To further achieve rational multi-target combination, we devised a combination strategy guided by the synergy coefficient q using the developed dual-target synergistic screen (Fig. 6a). Initially, q was calculated by comparing pairwise combinations with those containing individual targets based on indigoidine levels. Subsequently, an interaction map was constructed to identify targets within the positive synergetic. Guided by this map, we engineered the targets that

https://doi.org/10.1038/s41467-025-57073-5

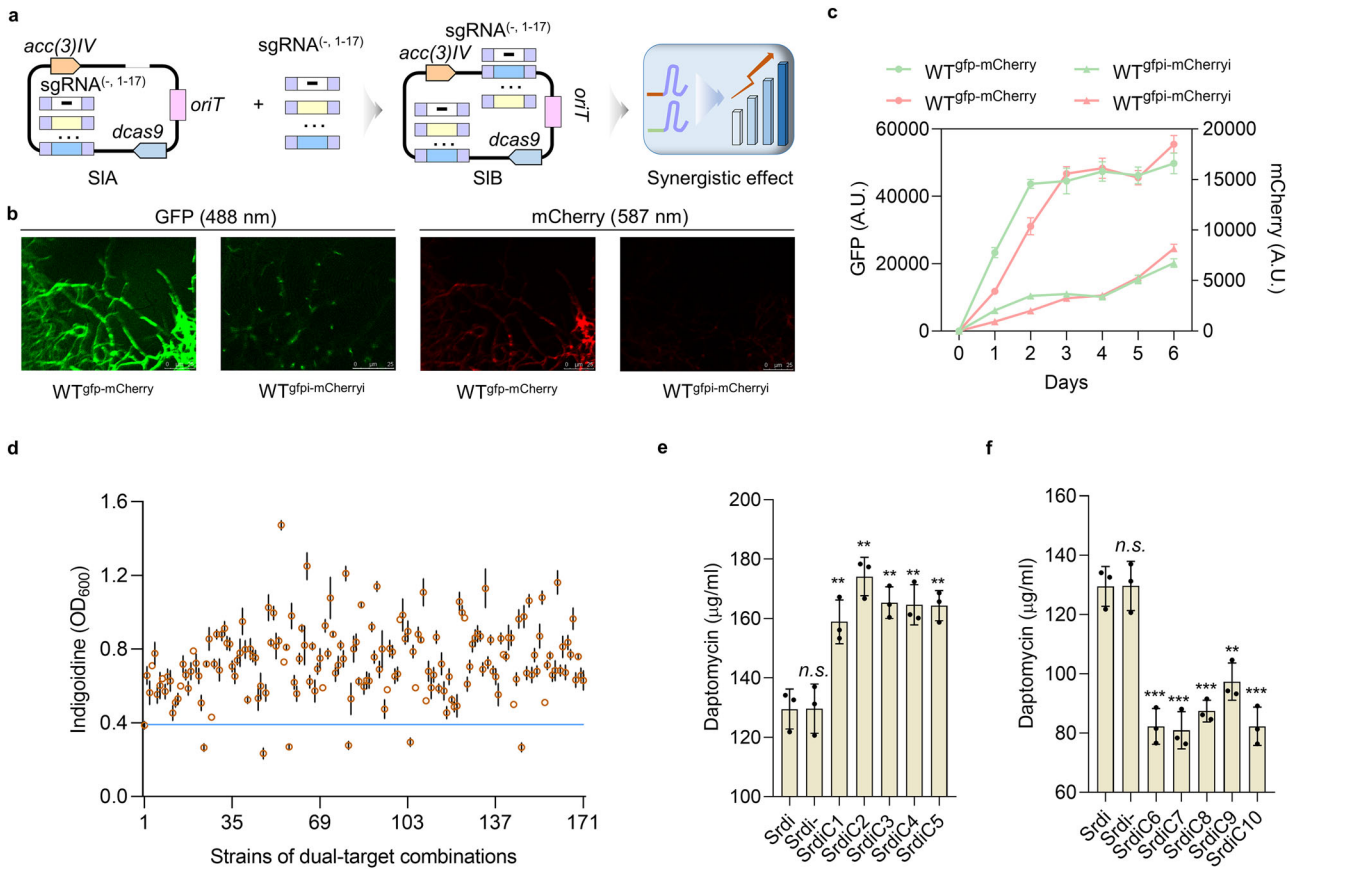

Fig. 5 | Development of a dual-target synergistic screening strategy. **a** Schematic illustrating the construction of a synergetic library, where SIA represents the single-target library and SIB denotes the synergistic library designed for simultaneous inhibition of two target genes. **b** Expression and inhibition of *gfp* and *mCherry* genes in *S. roseosporus* determined by laser confocal microscopy. $WT^{gfp\text{-}mCherry}$: WT expressing both *gfp* and *mCherry*. $WT^{gfpi\text{-}mCherryi}$: CRISPRi-mediated inhibition of *gfp* and *mCherry* in the $WT^{gfp\text{-}mCherry}$. The excitation wavelengths of GFP and mCherry are 488 nm and 587 nm, respectively. **c** GFP (green) and mCherry (red) fluorescence curves of $WT^{gfp\text{-}mCherry}$ and $WT^{gfpi\text{-}mCherryi}$ during a 6-day culture period. **d** Indigoidine level of 171 dual-target combinations correspond to 600 single colonies. The brown circle indicates the mean distribution, and the black dash indicates the standard deviation. The blue line indicates the indigoidine levels in the control strain Srdi⁻. **e** Daptomycin titer in strains (SrdiC1 through SrdiC5) exhibiting the five highest levels of indigoidine, as well as in control strains Srdi and Srdi⁻. [$p = 0.982953367$, 0.006952983, 0.00115138, 0.001932551, 0.003069223, 0.002012816 (left to right)]. **f** Daptomycin titer in strains (SrdiC6 through SrdiC10) with lower indigoidine levels than the control strains Srdi and Srdi⁻. [$p = 0.982953367$, 0.000820299, 0.000797634, 0.000673364, 0.003788098, 0.00092792 (left to right)]. Data in (**c**, **e**, **f**) are shown as the mean ± SD ($n = 3$ biological replicates). Two-tailed Student's *t* test was used in (**e**, **f**) to analyze the statistical significance (*n.s.* not significant ($p > 0.05$); $^{**}p < 0.01$; $^{***}p < 0.001$).

exhibited positive synergetic effects with each other. Here the value of *q* calculated by Jin's formula[35], which is a well-established approach for estimating the combined effect of two drugs on cellular pathological phenotypes[21]. Similarly, our focus was on investigating the synergistic effects between independent targets in relation to daptomycin synthesis phenotype.

We determined the *q* values of each pairwise combination of the identified targets (Supplementary Fig. 5a and Supplementary Table 2). These calculated *q* values were used to indicate antagonism ($q < 0.85$), additivity ($0.85 \le q < 1.15$), and synergism ($q \ge 1.15$). Among these combinations, we observed antagonism in a total of 62 pairs, while additivity was found in 70 combinations, and synergy was displayed in 21 combinations (Fig. 6b). Furthermore, through mapping the interactions among these targets, we discovered that all pairwise interactions involving *idt3*, *idt5*, *idt9*, and *idt15* demonstrated synergistic effects (Fig. 6c and Supplementary Fig. 5b).

To validate this finding, we constructed the strains inhibiting three out of these four targets in various combinations, as well as a strain simultaneously repressing all four targets. Upon comparing them to strains harboring each pairwise combination of the four targets individually, we found that all the three-target combinations exhibited significantly enhanced daptomycin titers, thereby confirming their positive synergistic effect (Fig. 6d). Notably, the strain carrying the four-target combination (denoted Sr11) achieved the highest daptomycin titer at 389 μg/mL in shake flask, representing an approximately 1.61-fold increase compared to WT (Fig. 6d). Conversely, random multi-target combinations (i.e., *idt4*, *idt7*, *idt11*, and *idt12*) exhibiting antagonism or additivity resulted in significantly lower or no significant difference in daptomycin titers (Supplementary Fig. 5c). These results highlighted the effectiveness of our synergy coefficient-guided combination strategy.

To test the production performance of the four-target combination in fed-batch condition, we conducted fermentation in a 7.5-L fermenter with sodium decanoate precursor feeding at 48 h and dextrin supplementation from 3 to 7 days (Supplementary Fig. 5d). Over a ten-day fermentation period, we found that daptomycin titer of Sr11 reached 1054 mg/L, which was two-fold higher than that of WT strain under the fed-batch condition, while both strains exhibited similar growth patterns throughout the fermentation process (Fig. 6e and Supplementary Fig. 5e).

To elucidate the underlying synergistic mechanism, we conducted comparative transcriptomics studies of the strains individually repressing these four targets (WT^{idt3i}, WT^{idt5i}, WT^{idt9i}, and WT^{idt15i}), as well as the four-target combination strain Sr11. Compared with the

https://doi.org/10.1038/s41467-025-57073-5

control strain WT-, a total of 931, 316, 581, 328, and 2437 differentially expressed genes were identified in WT^{idt3i}, WT^{idt5i}, WT^{idt9i}, WT^{idt15i}, and Sr11, respectively (Supplementary Fig. 6a). Sr11 exhibited a broader range of genetic perturbations compared to other strains and resulted in comprehensive integration that encompassed the majority of differentially expressed genes associated with *idt3*, *idt5*, *idt9*, and *idt15* inhibition. Functional clustering analysis revealed that the integrated differentially expressed genes in Sr11 play roles in remodeling multiplexed metabolic pathways such as biosynthesis of amino acids, biosynthesis of cofactors, quorum sensing, and nitrogen metabolism (Supplementary Fig. 6b). This integration was particularly evident in the upregulation of daptomycin BGC by approximately 15-26 fold in Sr11 (Fig. 6f). Furthermore, the time-course analysis demonstrated that individual inhibition of *idt3*, *idt5*, *idt9*, and *idt15* led to growth stage-

Fig. 6 | Synergistic multi-target engineering for improvement of daptomycin production. a Schematic of rational multi-target combination based on pairwise synergetic screening. **b** Interactions of 17 repressors involved in daptomycin synthesis. The synergy coefficient *q* value represents the ratio of the actual measured value of indigoidine to the expected value (assuming that the effects of the two genes on yield are independent events). When $q < 0.85$, indicates antagonism; $0.85 \le q < 1.15$, indicates additivity; and $q \ge 1.15$, indicates synergism. **c** Interactions network between targets based on synergy coefficient. Red dots indicate four targets that have a synergistic relationship with each other. Other targets are indicated by blue dots. **d** Daptomycin titer of WT (column 1), WT^{-} (column 2), and CRISPRi array-mediated strains. "+" indicates the use of CRISPRi to inhibit the corresponding gene, while "−" indicates no inhibition. Two-tailed Student's *t* test (*n.s.* not significant ($p > 0.05$); $^{**}p < 0.01$; $^{***}p < 0.001$). [$p = 0.900351215$, 0.000191464, 0.001315463, 0.000379374, 0.000513844, 0.001715257, 0.003379535, 7.1047E−05, 5.99658E−05, 0.000115786, 0.000141011, 1.92672E−05 (left to right)]. **e** Growth and daptomycin production curves of WT and Sr11 in a 7.5L fermenter. Biomass is quantified as dry cell weight. **f** Heat map of *dptE* operon transcription levels in WT^{idt3i}, WT^{idt5i}, WT^{idt9i}, WT^{idt15i}, and Sr11. **g** Transcription profile of daptomycin BGC in WT^{idt3i}, WT^{idt5i}, WT^{idt9i}, WT^{idt15i}, and Sr11 grown in fermentation medium. Here we selected *dptE* gene for quantification using RT-qPCR. Data in (**d**, **e**, **g**) are shown as the mean ± SD ($n = 3$ biological replicates).

specific upregulation pattern of daptomycin BGC; however, the four-target combination displayed a synergistic effect throughout the entire fermentation period (Fig. 6g). These findings underscored the achievement of our developed multi-target combination strategy in enhancing daptomycin production by harnessing synergistic pleiotropic effects of multiplex regulators.

Synergistic multi-target engineering for thaxtomin A and surfactin production

To investigate the applicability of our multi-target combination strategy in other NRP-producing *Streptomyces* species, we applied the developed analog co-expression and co-biosynthesis reporter system along with the multi-target synergistic combination approach to enhance the titer of thaxtomin A in heterologous host *S. coelicolor* M1152 (Fig. 7a). We integrated the thaxtomin BGC (*txt*) and *txt* with *idgS-sfp* cassette inserted after the stop codon of *txtB* into the genome of M1152 to generate two strains: Scotxt as a control strain and Scotxti as a reporter strain (Fig. 7a). However, both strains failed to produce detectable levels of thaxtomin A when cultured in ISP4 liquid media (Fig. 7c). Transcription analyses revealed that the *txt* gene cluster was cryptic in both Scotxt and Scotxti. Therefore, we decided to screen for the repressors capable of inhibiting thaxtomin A production, aiming to harnessed these repressor combinations to boost the titer of thaxtomin A in *S. coelicolor*.

We designed a pool of sgRNAs targeting 856 regulatory genes in *S. coelicolor* genome, with three sgRNAs targeting distinct sites on the NT strand of each gene. Similar to the screening conducted for inhibiting daptomycin biosynthesis, we identified 10 targets for inhibiting thaxtomin A. They are *sco5803* (named as *thaR1*), *sco5231* (*thaR2*), *sco3226* (*thaR3*), *sco4230* (*thaR4*), *sco3818* (*thaR5*), *sco5862* (*thaR6*), *sco1596* (*thaR7*), *sco2794* (*thaR8*), *sco1745* (*thaR9*), and *sco0204* (*thaR10*). Transformants inhibiting these targets all exhibited activation of thaxtomin A production (Fig. 7c).

To further elucidate the interaction among these targets, we constructed a pairwise combinatorial library comprising these identified target genes. The synergy coefficient *q* based on indigoidine levels was evaluated for all the combinations of the identified targets (Supplementary Fig. 7a). Among these combinations, antagonism was observed in a total of 25 pairs, while additivity was found in 19 combinations, and synergy was displayed in 11 combinations (Supplementary Fig. 7b). By mapping the interactions among these targets, we discovered that all pairwise interactions involving *thaR4*, *thaR7*, and *thaR8* showed positive synergistic effects (Fig. 7c and Supplementary Fig. 7c).

The engineered strains carrying the combinations of these targets all demonstrated a significant increase in thaxtomin A production (Fig. 7d). Notably, thaxtomin A titer reached a very high level of 352 mg/L in shake flask for the three-target combination strain (referred to as Scotxt4, Fig. 7d). These results not only demonstrated the successful heterologous activation of thaxtomin A in *S. coelicolor*, but also showcased the efficacy of our multi-target combination strategy in augmenting NRPs titers across diverse *Streptomyces* backgrounds.

To further test the broad applicability, we employed the synergistic multi-target engineering strategy to enhance surfactin production in *B. subtilis* 168 (Fig. 7a). We initially activate the biosynthesis of surfactin by integrating *sfp* gene from *Bacillus amyloliquefaciens* MT45 to generate 168S1 with surfactin titer of 225 mg/L (Fig. 7e). Subsequently, we inserted *idgS-sfp* cassette downstream of the stop codon of *srfAD* (Fig. 7a) and screened the repressors of surfactin biosynthesis similar to that of daptomycin and thaxtomin A. We identified 11 repressors (*bsu_03880* (*srfR1*), *bsu_40300* (*srfR2*), *bsu_11500* (*srfR3*), *bsu_06830* (*srfR4*), *bsu_16170* (*srfR5*), *bsu_37460* (*srfR6*), *bsu_00370* (*srfR7*), *bsu*_08730 (*srfR8*), *bsu_03770* (*srfR9*), *bsu_13310* (*srfR10*), and *bsu_24600* (*srfR11*)), and further validated that inhibition of these targets demonstrated significant activation of surfactin production (Fig. 7e). Then we determined the interaction map of these repressors by *q* value (Fig. 7f and Supplementary Fig. 8a, b). The interaction map indicated that all pairwise interactions involving *srfR1*, *srfR5*, *srfR7*, and *srfR10* displayed positive synergy (Fig. 7f and Supplementary Fig. 8c). As expected, engineered strains carrying combinations of these synergistic targets showed improvement of surfactin titer to 878 mg/L in shake flask cultures, which was nearly 4 times higher than the strain 168S1. These results again evidenced the effectiveness of our rational multi-target combination strategy in enhancing NRP titers across diverse species.

Discussion

The excellent traits of organisms are the result of synergistic interactions among multiple genes[36], and similarly, the high-yield traits of bacteria are not solely determined by individual genes but rather the outcome of intricate interactions among multiple targets[37]. Progress in strain engineering has demonstrated that most enriched mutations or recombination events synergistically increase titers by hundreds or thousands of times greater than that of the original isolated strain[38]. One impressive example is the strain improvement program for penicillin production, where a series of successive screenings and enrichment of favorable mutations has led to a titer increase from 0.06 g/L to over 100 g/L over the past 80 years[39]. However, this process involving generating millions of mutations, and testing each mutant strain to select phenotypes with increased production is labor-intensive and inefficient[40]. To achieve accurate and efficient manipulation of multiple favorable targets, we developed a screening-based rational multi-target combination strategy and significantly improved the titers of daptomycin, thaxtomin A and surfactin in *S. roseosporus*, *S. coelicolor* and *B. subtilis*, respectively. Our work demonstrated that understanding the complex interactions is essential for advancing the knowledge of multi-target combination and then harnessing these synergistic effects to rapidly improve microbial cell factory performance.

Strain engineering often relied on combining multiple desired targets; however, not all combinations proved effective. For instance, both redox-response regulators RshA and CosR repressed nanobody VHH production in *Corynebacterium glutamicum*, but double mutant strains exhibited less titer increase compared to the individual mutants[9]. Similarly, another study identified 56 genes and

https://doi.org/10.1038/s41467-025-57073-5

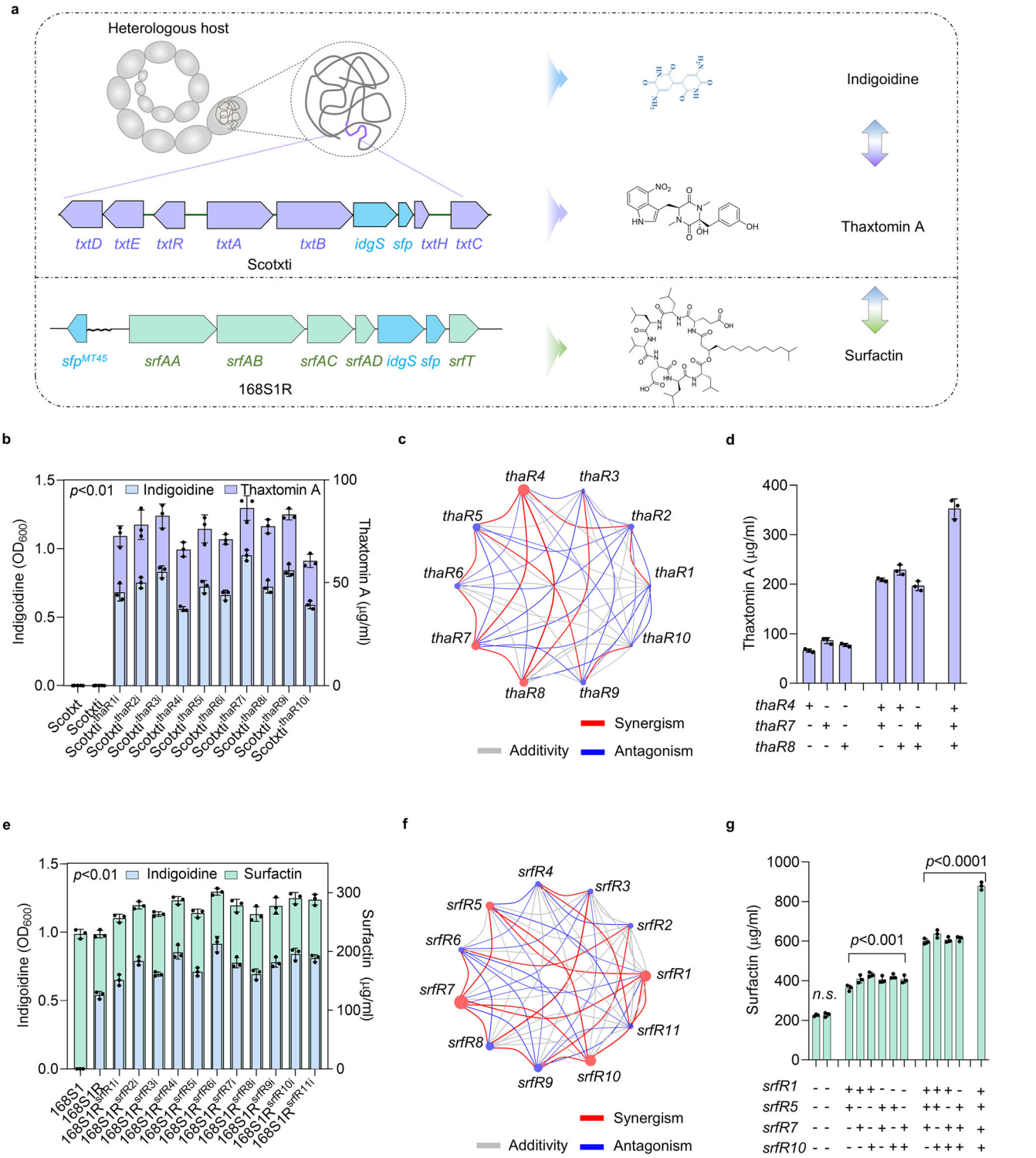

corresponding sgRNAs beneficial for promoting free fatty acids (FFAs) production in *Escherichia coli*; however, when combined the high-yielding strain (*ihfA*$^{L-}$-*aidB*$^{+}$) with each of the beneficial sgRNAs, only 6 combinations further improved FFAs production[8]. Therefore, previous multi-target combination approaches relied on subjective trial-and-error processes that were time-consuming and often led to inferior outcomes compared to single-target operations. In this work, we propose exploring the synergistic interaction of multiplex targets involved in NRP biosynthesis, and then rationally guiding the construction of high-yielding strains through multi-target combination. To map the interplay of multi-targets from the data of dual-target screening, we introduced *q* value used in drug synergy screening to evaluate the synergistic effects on the yield phenotype[41]. Based on the *q* value, we obtained the interplay map of all the targets. As we expected, combinations of targets with synergistic relationships effectively improved production yield while those with antagonistic relationships had no such effect (Fig. 6d and Supplementary Fig. 5c). Moreover, we demonstrated that our selected four-target combination indeed synergistically promoted daptomycin production at the transcriptional level (Fig. 6f, g). These data demonstrated effectiveness of synergistic screening in strain improvement efforts. Thus, mapping global regulator interactions to elucidate high-yielding phenotype will

Fig. 7 | Synergistic multi-target engineering for improvement of thaxtomin and surfactin production. a Schematic diagram of increased thaxtomin and surfactin production by the analog co-expression and co-biosynthesis reporter system. The promoterless reporter genes *idgS-sfp* are fused downstream of *txtB*, resulting in an overlap between the TGA stop codon of *txtB* and the ATG start codon of *idgS*. The codon-optimized reporter genes *idgS-sfp* are fused downstream of *srfAD*, resulting in an overlap between the TGA stop codon of *srfAD* and the ATG start codon of *idgS*. **b** Indigoidine level and thaxtomin A titer when inhibiting the identified targets in Scotxti. [p = 4.65485E−05, 5.35998E−06, 5.04019E−06, 6.08803E−07, 1.08422E−05, 5.02854E−06, 2.08711E−06, 1.08422E−05, 4.80512E−06, 4.43093E−06 (indigoidine: left to right); p = 1.4452E−05, 4.57848E−05, 1.64923E−05, 5.12443E−06, 4.2004E−05, 8.81769E−07, 1.55787E−05, 2.38202E−06, 6.58047E−07, 5.21529E−06 (thaxtomin A: left to right)]. **c** Interactions network between targets based on synergy coefficient. Red dots indicate four targets that have a synergistic relationship with each other. Other targets are indicated by blue dots. **d** Thaxtomin titer of CRISPRi-mediated strains. "+" indicates the use of CRISPRi to inhibit the corresponding gene, while "−" indicates no inhibition. **e** Indigoidine level and surfactin titer when inhibiting the identified targets in 168S1R. [p = 0.016500953, 0.000413121, 0.000963969, 0.00063344, 0.001814368, 0.000499214, 0.0008904, 0.004535417, 0.000745307, 0.000522386, 0.000235722 (indigoidine: left to right, control:168S1R); p = 0.953066195, 0.010555248, 0.00110127, 0.002547204, 0.000626228, 0.00415879, 0.000214603, 0.003250768, 0.016483722, 0.006590528, 0.00105454, 0.001113834 (surfactin: left to right, control:168S1)]. **f** Interactions network between targets based on synergy coefficient. Red dots indicate four targets that have a synergistic relationship with each other. Other targets are indicated by blue dots. **g** Surfactin titer of CRISPRi-mediated strains. "+" indicates the use of CRISPRi to inhibit the corresponding gene, while "−" indicates no inhibition. [p = 0.722658162, 0.000105794, 0.000105702, 9.6318E−06, 6.99555E−05, 1.3685E−05, 0.000100527, 1.62203E−06, 4.15269E−06, 1.64117E−06, 8.92386E−07, 6.09771E−07 (left to right)]. Data in (**b**, **d**, **e**, **g**) are shown as the mean ± SD (n = 3 biological replicates). Two-tailed Student's t test was used in (**b**, **e**, **g**) to analyze the statistical significance (n.s. not significant ($p > 0.05$); $^{**}p < 0.01$; $^{***}p < 0.001$; $^{****}p < 0.0001$).

hold great potential for the construction of efficient microbial cell factory.

We focused on regulators of *S. roseosporus* as they play a crucial role in orchestrating the global metabolism and related physiological events through diverse interactions within the transcription regulatory network[30]. Our screen aimed to identify potential repressors, considering that SM biosynthesis is triggered under specific environmental conditions and growth stages, involving a multitude of repressors in cross-regulation[5]. In this study, we identified 17 regulators that directly or indirectly inhibit daptomycin production. Previously, identifying repressors located outside of daptomycin BGC has been challenging due to methodological limitations, and thus far only four have been reported (DepR2[42], PhaR[43], WblA[33], DasR[32]), of which WblA was also included in our screening results. For thaxtomin A and surfactin, we screened 10 and 11 negative regulatory proteins, respectively (Fig. 7b, e). Our study highlights the existence of numerous unknown repressors involved in regulation of NRPs diverse species, which necessitates further exploration using our developed efficient identification strategy. Furthermore, we designed a workflow to investigate the interactions between these identified repressors in relation to NRP production, and rationally combined the synergistic targets. Therefore, the workflow of identifying regulators and exploring their interactions provides a feasible rational strategy for developing high-yield strains with multi-target modification.

Numerous studies have demonstrated that genes with similar expression profiles are often functionally related and vice versa[44]. Especially, the production of SMs in *Streptomyces* involves in the synergistic effect of multifaced metabolic and physicological regulators[29]. Our developed reporter system, characterized by the co-expression and co-biosynthesis of the reporter indigoidine and the desired NRPs, enables genome-wide screening for these regulatory targets. Since both the reporter compound and the desired products belongs to NRP type SMs and were biosynthesized by a multi-module enzyme assembly line, indigoidine BGC could be considered as an additional BGC module of daptomycin or thaxtomin A in our reporter system design (Fig. 2a). Such design ensured the identification of targets that not only contribute to the expression of daptomycin BGC and its related genes, but also the targets that commonly benefit for such NRP compound biosynthesis (Fig. 2b–d). Previously, a reporter-guided mutant selection (RGMS) method was initially used to improve lovastatin production in *Aspergillus terreus*[45] and subsequently improved through double-reporter-guided mutant selection to enhance clavulanic acid production in *Streptomyces clavuligerus*[46]. However, these studies utilized reporters that were genes conferring antibiotic resistance or enzymes catalyzing color reactions rather than achieving co-transcription and co-biosynthesis of an analog reporter compound belonging to the same class. To the best of our knowledge, our findings provided unequivocally evidence for the first time that the expression level of BGCs can serve as a representative indicator for a group of functionally related genes that collectively coordinate biosynthesis (Fig. 2f, g). We believe that this screening strategy can also be applied to the high-yield phenotype screening of other colorless NRPs.

Expression of SM BGCs in heterologous hosts amenable to industrial-scale fermentation can lead to higher yield. By implementing heterologous production of herbicide thaxtomin A in *S. coelicolor*, we demonstrated the efficiency of this screening-based rational multi-target combination strategy: not only were we able to activate the silent thaxtomin A BGCs in *S. coelicolor*, but we also increased the titer of thaxtomin A to an exceptionally high level (Fig. 7e). Given that genetic background incompatibility between a heterologous host and desired BGC is a common issue[23], our screening-based rational multi-target combination strategy provides a feasible one-stop solution for activating cryptic NRP BGCs and subsequently improving their titers.

High-throughput CRISPR-based technologies facilitate rapid generation of extensive variant libraries, such as simultaneous inhibition or activation, or concurrent inhibition of one gene while activating another in pairwise fashion, thereby providing enhanced possibilities for synergistic screening[47]. However, the application of CRISPR-mediated synergistic screening remains unexplored in strain improvement. In this study, we developed a synergistic CRISPRi library to simultaneously inhibit the expression of dual targets and investigated genetic interactions of identified regulators involved in inhibition of daptomycin and thaxtomin A production in different *Streptomyces* strains. Our findings highlight the potential utilization of widely-used CRISPR technology as a priority manipulation tool for collaborative multi-target research in *Streptomyces* species.

The strain Sr11, which exhibits synergistic effects on four targets, achieved daptomycin titers of 389 mg/L in shake flasks and to 1054 mg/L in a 7.5-L fermenter. These results surpass previous reported highest yields in shake flasks (350 μg/mL)[48] and fermenters (812 μg/mL)[25]. Despite the significant increase in daptomycin yield, no metabolic burden was observed during growth (Fig. 6e). We hypothesize that this lack of burden could be due to the relatively low carbon yield of SMs, which typically accounts for less than 1% of total carbon flux. Specifically, Sr11 exhibited a carbon allocation of approximately 0.6%, while the WT strain showed about 0.2%. Given that SMs such as daptomycin are produced in much smaller quantities relative to bulk chemicals, our synergistic effect of the four targets combination may not have been sufficient to induce a noticeable growth burden. Additionally, the rich media used in fermentation could masked any potential metabolic burden, which might become more evident in selective media. To confirm this conjecture, we compared the extracellular by-products (Supplementary Fig. 5e) and intracellular concentrations of 14 amino acids (Supplementary Fig. 5f)

between the final strain Sr11 and WT. The results showed no significant differences, suggesting that the strain's robustness could be maintained to some extent.

Collectively, we developed a screening-based rational multi-target combination strategy for improving the titers of NRPs. The framework of this strategy encompasses the CRISPRi-mediated disturbance of individual target or pairwise combination, the analog co-expression and co-biosynthesis reporter system-based screening, and the mapping of cooperativity-based interaction relationships. By employing this strategy, we readily engineered multiplex targets with synergistic effect and achieved titers of daptomycin, thaxtomin A and surfactin to 1054 mg/L in 7.5-L fermenter, 352 mg/L and 878 mg/L in shake flask in *S. roseosporus*, *S. coelicolor* and *B. subtilis*, respectively. Our developed screening-based rational multi-target combination strategy and workflow hold potential for future strain engineering endeavors.

Methods

Strains, plasmids, primers, and growth conditions

Strains and plasmids used in this study are listed in Supplementary Table 3, and primers and sgRNAs are listed in Supplementary Table 4. *S. roseosporus* NRRL11379 (WT) and its derivatives were grown at 28 °C on solid DA1[49] for sporulation and phenotype observation. *S. coelicolor* M1152 and its derivatives were grown at 28 °C on solid MS[50] for sporulation. Solid RM14 medium was used for protoplast regeneration[49]. For daptomycin titer, seed medium and fermentation medium[49] were used. For thaxtomin titer, liquid TSB and ISP4 medium were used[23]. *E. coli* JM109, NEB 10-beta (Biomed; Beijing, China), and ET12567 (*dam dcm hsdS*)[30] were grown at 37 °C in Luria-Bertani (LB) medium and used for DNA cloning, library construction, and propagation of non-methylated DNA for transformation into *Streptomyces* strains, respectively. *B. subtilis* 168 and its derivatives were grown at 37 °C on LB medium. Fermentation medium (6.5% sucrose, 0.8% NH_4NO_3, 0.03 M KH_2PO_4, 0.04 M Na_2HPO_4, 7 μM $CaCl_2$, 4 μM $FeSO_4$, 100 μM $MgSO_4$, 4 μM ethylene diamine tetra-acetic acid) was used for fermentation experiments.

Construction of S. roseosporus, S. coelicolor and B. subtilis mutant strains

To investigate *idgS* expression in *S. roseosporus*, plasmid pSET-dptEp-idgSsfp was constructed by ligation of *dptEp* (amplified from WT DNA with primers YH104A/YH104B) and *idgS-sfp* (amplified from pCIMt005[51] with primers YH105A/YH105B) fragments into *Eco*RI-digested integrative plasmid pSET152[52] using Gibson assembly method. Similarly, pSET-ermE*p-idgSsfp was constructed by ligation of *ermE*p* (amplified from pObldD[30] with primers YH106A/YH106B) and *idgS-sfp* (amplified with primers YH107A/YH107B) into pSET152. The two plasmids were then introduced into WT protoplasts, respectively, resulting in strains WT/pSET-dptEp-idgSsfp and WT/pSET-ermE*p-idgSsfp.

To construct reporter strain Srdi, two fragments flanking the *dptD* stop codon were amplified from WT DNA with primers YH108A/YH108B and YH110A/YH110B, and *idgS-sfp* fragment was amplified from pCIMt005 with primers YH109A/YH109B. *dptD* 5′-flanking region, *idgS-sfp*, and 3′-flanking region were assembled into *Eco*RI-digested pKC1139[52] to generate pKC-Srdi, which was then transformed into WT protoplasts. Transformants on RM14 regeneration medium were transferred to DA1 plates for sporulation. Double-crossover mutant Srdi was screened by homologous double exchange, verified by PCR analysis with primers YH111A/YH111B and YH112A/YH112B, followed by DNA sequencing.

The mutant strains with premature introduction of a stop codon were constructed by CRISPR-cBEST system[53]. To construct *tetR6* or *tetR7* deletion mutants, the corresponding sgRNA harboring the specific spacer was amplified from pKCCpf1[54] by primers YH131A/YH131B and YH136A/YH136B and then ligated into *Spe*I/*Nde*I-digested pKCCpf1. 5′- and 3′-flanking regions of *tetR6* were amplified with primers YH129A/YH129B and YH130A/YH130B, and those of *tetR7* were amplified with primers YH134A/YH134B and YH135A/YH135B, and then respectively ligated into *Hin*dIII-digested pKCCpf1 with corresponding sgRNA using Gibson assembly to generate pCpf1ΔtetR6 and pCpf1ΔtetR7, which were transformed into WT protoplasts. The double-crossover mutants ΔtetR6 and ΔtetR7 were selected and verified by PCR analysis using primer pairs YH132A/YH132B and YH133A/YH133B (for ΔtetR6), or YH137A/YH137B and YH138A/YH138B (for ΔtetR7), followed by DNA sequencing.

The reporter gene *idgS-sfp* was transferred into pSET152::*txt*[23] via λ-Red-mediated recombination[23], named pSET152::*txt-idgSsfp*. The plasmids pSET152::*txt* and pSET152::*txt-idgSsfp* were then introduced into *S. coelicolor* M1152 protoplasts, respectively, resulting in strains Scotxt and Scotxti.

To construct 168S1, two fragments about 1.1 kb upstream and downstream of the *sfp* (*bsu_03570*) gene was amplified from *B. subtilis* 168 with primers YH203A/YH203B and YH205A/YH205B, and sfp^{MT45} fragment was amplified from *B. amyloliquefaciens* MT45 with primers YH204A/YH204B. Three fragments were assembled into *Eco*RI/ *Bam*RI-digested pKSV7[55] to generate pKS-sfp^{MT45}, which was then transformed into *B. subtilis* 168 competent cells. The mutant 168S1 was obtained after two rounds of crossover and verified with primers YH206A/YH206B. To further construct reporter strain168S1R, two fragments flanking *srfAD* stop codon were amplified from WT DNA with primers YH207A/YH207B and YH209A/YH209B, and codon-optimized *idgS-sfp* fragment (codon optimization and gene synthesis by GENEWIZ Co., Ltd) with primers YH208A/YH208B. *srfAD* 5′-flanking region, *idgS-sfp*, and 3′-flanking region were assembled into *Eco*RI/ *Bam*RI-digested pKSV7[55] to generate pKS-Bsudi, which was then transformed into 168S1 competent cells. Double-crossover mutant 168S1R was screened and verified by PCR analysis with primers YH210A/YH210B. *B. subtilis* 168 was transformed using the Spizizen method[56].

Fermentation and analysis of daptomycin titer

Spores from different *S. roseosporus* strains, grown on DA1 plates for 7 days, were transferred to 250 mL flasks containing 50 mL of primary seed medium and incubated at 28 °C for 48 h on a rotary shaker set at 250 rpm. The primary seed culture was then used to inoculate 50 mL of secondary seed medium at a 5% (vol/vol) inoculum, and the culture was further incubated at 28 °C with shaking for 30 h. Afterward, 5% (vol/vol) of the secondary seed culture was transferred into 50 mL of fermentation medium, and fermentation continued for 10 days. During the fermentation process, sodium decanoate was added every 12 h at a final concentration of 0.02% (wt/vol) after the first 48 hours, continuing until the fermentation was completed. The fermentation broth (1.0 mL) was centrifuged at 12,000 × *g* for 10 min. The resulting supernatant was filtered using a 2.2 μm membrane filter, and the filtrate was directly injected into an HPLC system (model 600; Waters, Milford, CT) equipped with a C18 column (4.6 mm × 250 mm). The mobile phase consisted of 0.1% trifluoroacetic acid in water and acetonitrile (55:45, vol/vol), with a flow rate of 1.0 mL/min. Daptomycin was detected by UV absorbance at 218 nm, and its concentration was quantified using standard curves generated with authentic daptomycin samples (Shanghai Qiao Chemical Science, China).

Fermentation in a 7.5-L fermenter (New Brunswick, BioFlo®/CelliGen®115) was performed at 28 °C with an initial culture volume of 3.0 L. Inoculation was 5% (v/v) and the aeration rate was controlled at 3.0 vvm. Dissolved oxygen (DO) was maintained above 20% of the saturated dissolved oxygen concentration by adjusting the agitation speed above 200 rpm. Aqueous solution containing 2% (w/v) sodium decanoate precursor was added at the rate of 40 μL/min after 48 h, and dextrin was supplemented at a flow rate of 25 mg/min during day 3 (when reducing sugar and total sugar contents dropped to 3 g/L and 20 g/L) to day 7. During the fermentation process, biomass was

determined by dry cell weight from 80 °C for 24 h, and pH value was maintained at 6.5 with 25% NH_4OH.

Fermentation and analysis of thaxtomin A titer

For thaxtomins production, *S. coelicolor* spores were inoculated in liquid TSB and incubated for 48 h as a seed culture, and then 2.5 mL of each seed culture was transferred into a shake flask containing 50 mL ISP4 with 1% cellobiose[23]. HPLC analysis of thaxtomin A titer was performed with a SGIMADZU LC-20A HPLC system and a ZORBAX SB-C18 column (5 µm pore size; 4.6 by 250 mm).

Fermentation and analysis of surfactin titer

For surfactin production, *B. subtilis* 168 and its derivatives were precultured in LB medium and then incubated at 37 °C with shaking at 200 rpm for 16 h as seed cultures. Five milliliters of seed culture was inoculated into 50 mL of fermentation medium in a 250 mL flask and cultured at 37 °C with shaking at 200 rpm for 48 h. To determine surfactin, the cell-free culture broth was adjusted to pH 2.0 with 6 M HCl, then centrifuged at 10,000 × *g* for 30 min. The supernatant was discarded, and the pellet was re-dissolved in 100% methanol to obtain crude surfactin. The surfactin quantification was carried out using a Waters UPLC H-class system, which included a binary solvent delivery system and an auto-sampler. Chromatographic separation was achieved on a Waters Acquity C18 column (50 mm × 2.1 mm, 1.7 µm particle size), with a 5 µL injection volume. The mobile phase consisted of solvent A (HPLC-grade water with 0.1% formic acid) and solvent B (HPLC-grade methanol). A linear gradient elution from 85% to 100% solvent B over 6 min was applied at a flow rate of 0.3 mL/min. The elution profile was monitored by measuring absorbance at 215 nm. The surfactin concentration was calculated and quantified using Empower Version 3.0 software[57]. The total surfactin concentration was the sum of the concentrations of four homologs. Surfactin standards were purchased from Sigma (St. Louis, MO, USA). All experiments were conducted in triplicate.

GC-MS analysis

GC-MS was used to identified relative level of intracellular amino acids analysis. The GC–MS system (Agilent) employed for the analysis consisted of a 7890 GC, a 5975 MS, and a 7683 auto-sampler, with a HP-5 MS capillary column (30 m × 250 µm × 0.25 µm, J&W Scientific). For metabolomic profiling, 1 µL of the sample was injected with a 1:10 split ratio. The temperature program started at 70 °C for 1 minute, then ramped at 5 °C/min to 230 °C, followed by an increase of 10 °C/min to 290 °C, and was held at 290 °C for 6 min. Ions were produced using the 70 eV electron beam at a 40 µA ionization current, and the mass spectrum was recorded in the range of 50–650 m/z. For amino acid analysis, 1 µL of the sample was injected with a 1:30 split ratio. The chromatographic conditions were as follows: 70 °C for 2 minutes, then a temperature increase to 290 °C at 5 °C/min, which was held for 3 minutes. Helium was used as the carrier gas at a flow rate of 1.0 mL/min. Both the injector and detector temperatures were maintained at 290 °C.

Next-generation sequencing (NGS)

The DNA samples were amplified using primers YH139A/YH139B with plasmid library and transformants library as templates respectively. The NGS was carried out and analyzed by GENEWIZ Co., Ltd. on illumina Miseq.

Determination of sugar content

The concentration of reducing sugars and total sugars (acid hydrolysis) was determined by the 3,5-dinitrosalicylic acid (DNS) method[58].

Real-time RT-PCR (qRT-PCR) assay

S. roseosporus cells grown in liquid seed or fermentation medium and *S. coelicolor* cells grown in ISP4 liquid medium for 2 days were harvested for RNA extraction using the TRIzol method. Each RNA sample (4 µg) was treated with DNase I (TaKaRa; Japan) to digest genomic DNA, and then subjected to reverse transcription with M-MLV reverse transcriptase (Promega; USA). The cDNA obtained was used as template for qRT-PCR analysis (using primers listed in Supplementary Table 4). Relative expression level of tested genes was normalized with housekeeping gene 16S *rRNA* as the internal control using comparative Ct method. Expression value for each gene was determined in triplicate.

Quantitative assay of indigoidine production

S. roseosporus and *S. coelicolor* strains carrying *idgS-sfp* genes were cultured in liquid seed medium and ISP4 liquid medium for 3 days, and indigoidine production was measured by recording OD_{600} of the culture supernatants using multifunctional plate reader (Molecular Devices; USA). The supernatant of WT or plasmid control strain was used as a blank control.

Gene inhibition and base editing in *S. roseosporus*

Plasmid pSETdCas9Rg-2 for CRISPRi was constructed based on pSET-dCas9[59] and pKCcas9dO[59]. sgRNA expression element (*J23119p*-sgRNA-terminator) was amplified from pKCcas9dO with primers YH201A/YH201B and then assembled into *Eco*RI-digested pSET-dCas9 by Gibson assembly to generate pSETdCas9Rg. pSETdCas9Rg-2 backbone was amplified from pSETdCas9Rg with primers YH202A/YH202B to introduce two *Bsa*I cleavage sites between *J23119p* and sgRNA core scaffold. For gene inhibition, the oligo 5´-TAGT(N20)G-3´ and the reverse complement oligo 5´-AAAAC(N20)-3´were synthesized, annealed into double strands, and then ligated into *Bsa*I-digested pSETdCas9Rg-2 to generate CRISPRi plasmids.

CRISPR-cBEST plasmids for base editing were constructed based on pCRISPR-cBEST (Addgene #125689)[53]. The 20-nt spacer (N20) of sgRNAs was designed by software CRISPy-web (https://crispy.secondarymetabolites.org)[34]. For base editing, 5´-CGGTTGGTAG-GATCGACGGC(N20)GTTTTAGAGCTAGAAATAG-3´ and the reverse complement strand were synthesized, annealed, and assembled into *Nco*I-digested pCRISPR-cBEST by Gibson assembly to generate CRISPR-cBEST plasmids. The demethylated CRISPRi and CRISPR-cBEST plasmids from *E. coli* ET12567 were transformed into *S. roseosporus* protoplasts. 5–8 transformants were selected for sequencing to screen the correct constructs.

To obtain plasmid-free strains, the base-edited *S. roseosporus* strains containing CRISPR-cBEST plasmid were cultured at 37 °C on DA1 plates for plasmid curing. After incubation for 5 days, spores were spread on DA1 plates without apramycin and cultured at 28 °C for 5–7 days. Then, 15–20 colonies were separately inoculated onto apramycin-containing DA1 plates and those could not grow were plasmid-free.

Construction and analysis of the CRISPRi library and synergistic library

The sgRNA pool was used for targeted inhibition of 610 predicted regulatory genes in *S. roseosporus* and 856 regulator genes in *S. coelicolor* genome. All sgRNAs were designed to target the NT strand and 3 target sites were selected for each gene. The sgRNAs were synthesized as 108-nt oligonucleotides (ATCGGATCCTTGACAGCTAGCTCAGTCC TAGGTATAATACTAGT(N20)TTTTAGAGCTAGAAATAGCAAGTTAAAA TAAGGCTAGTCCGTTA), each consisting of the 20-nt sgRNA spacer sequence and 44-nt flanking region homolog to pSETdCas9Rg-2 backbone in *S. roseosporus* and pSETdCas9Rg-3 backbone in *S. coelicolor*. The sgRNA pool was designed and synthesized in batches by GenScript (Nanjing, China). Oligonucleotides were amplified by PCR with primers YH139A/YH139B. To minimize bias in the library, 15 cycles of amplification was used. The pSETdCas9Rg-2 backbone was amplified by PCR and then was digested with *Dpn*I. Amplified sgRNA oligonucleotides

were assembled into pSETdCas9Rg-2 or pSETdCas9Rg-3 backbone by Gibson assembly to construct CRISPRi plasmid library. To improve the coverage of the plasmid library, the library was independently constructed 20 times. The assembled product was sequentially transformed into *E. coli* NEB 10-beta, ET12567 and *S. roseosporus* Srdi or Scotxti. The resulting transformants were subjected to visual screening and sequencing analysis to determine the targeted genes.

For constructing the synergistic library, the CRISPRi plasmids of screened genes that inhibit daptomycin or thaxtomin production were separately constructed. The obtained CRISPRi plasmids and control plasmid pSETdCas9Rg-2/ pSETdCas9Rg-3 generated SlA library. The plasmid backbones and sgRNAs were both amplified from SlA library, and sgRNAs were then assembled into the other site of the SlA plasmid backbones i.e., between the resistance gene and the origin of replication, to generate synergistic library SlB (Fig. 5a). In addition to control plasmid, each SlB plasmid contained 1 or 2 sgRNAs. The SlB library was transformed into Srdi for synergistic screening based on indigoidine production. The SlA library was also transformed into reporter strain for calculating the synergy coefficient.

The CRISPRi library and synergistic library were constructed based plasmid pLCg6-dcpf1[60] (dCpf1 expression plasmid) and pcra3[60] (sgRNA expression plasmid) in *B. subtilis* 168. The yield of surfactin in 168S1R$^-$ (with empty plasmid pLCg6-dcpf1 and pcra3) was comparable to that of 168S1R. The pLCg6-dcpf1 was first transformed into 168S1R and inserted into *lacA* gene. To construct the CRISPRi library, all sgRNAs were designed to target the NT strand and 3 target sites were selected for each gene. The sgRNAs were synthesized as 27 oligonucleotides AGAT(N23) and AATT(N23(Reverse complementary sequence)). The oligonucleotides were annealed and ligated into *Eco*31I-digested pcra3. The synergistic library and multi-gene targeting plasmids were constructed by golden gate assembly[60]. All 66 combinations in the synergistic library (55 dual-target combinations and 11 single-targeting) were independently constructed.

Quantitative measurement of fluorescence intensity

S. roseosporus strains carrying corresponding plasmids were cultured in liquid seed medium. 10 mL culture was centrifuged, and resuspended in 1 mL Tris-HCl (20 mM, pH 7.5). The cell suspension was sonicated on ice for 5 min (pulse 3 s, stop 5 s), and the protein concentration in the supernatant was quantified with Bradford protein stain (Bio-rad, Quick Start™ Bradford 1× Dye Reagent). 200 µL protein solution with the same OD_{595} was used for fluorescence measurement by SpectraMax M3 microplate reader (Molecular Devices; USA). GFP abundance was quantified at an excitation wavelength of 488 ± 10 nm and an emission wavelength of 511 ± 10 nm. mCherry abundance was quantified at an excitation wavelength of 588 ± 10 nm and an emission wavelength of 644 ± 10 nm.

Fluorescence microscopy

5 µL of 3-day *S. roseosporus* culture in liquid seed medium was spotted onto a glass slide and a coverslip was put on the top. Mycelia were observed by confocal laser scanning microscopy (GFP excitation at 488 nm; mCherry excitation at 588 nm) (model TCS SP8, Leica Microsystems; Germany) with an oil-immersion objective.

Synergistic effect

The indigoidine level of each strain on day 3 was determined by multifunctional plate reader, with WT$^-$ as zero and Srdi$^-$ as blank control.

Synergistic effect was calculated by the Jin's formula:

$$q = \frac{E(A+B)}{EA+EB-E\text{control}}$$

Where E(A + B) and EA, EB are the average effects of simultaneous targeting of two genes vs. targeting two genes individually. In this method, $q < 0.85$ indicates antagonism, $0.85 \le q < 1.15$ indicates additivity, and $q \ge 1.15$ indicates synergism[35].

Statistics and reproducibility

Statistical analyses and data graphing were performed using GraphPad Prism (version 8.4.0) and Microsoft Excel (version 16.45). All statistical analyses performed reflect comparisons between distinct samples, rather than repeated measures. Statistical tests used in each experiment are indicated in their respective figure legends. Data are presented as means ± standard deviation (SD), and statistical significance between groups is assessed by *p*-values, denoted by asterisks ($^*p < 0.05$, $^{**}p < 0.01$, $^{***}p < 0.001$, $^{****}p < 0.0001$, and *n.s.* no significant difference). No statistical method was used to predetermine sample sizes.

Reporting summary

Further information on research design is available in the Nature Portfolio Reporting Summary linked to this article.

Data availability

All data associated with this study are present in the paper or the Supplementary Information. The NGS for library coverage generated in this study have been deposited in the NCBI Sequence Read Archive database under accession code PRJNA1220263. Source data are provided with this paper.

References

1. Li, J. W. & Vederas, J. C. Drug discovery and natural products: end of an era or an endless frontier? *Science* **325**, 161–165 (2009).
2. Harvey, A. L., Edrada-Ebel, R. & Quinn, R. J. The re-emergence of natural products for drug discovery in the genomics era. *Nat. Rev. Drug Discov.* **14**, 111–129 (2015).
3. Lacey, H. J. & Rutledge, P. J. Recently discovered secondary metabolites from *Streptomyces* species. *Molecules* **27**, 887 (2022).
4. Urem, M., Swiatek-Polatynska, M. A., Rigali, S. & van Wezel, G. P. Intertwining nutrient-sensory networks and the control of antibiotic production in *Streptomyces*. *Mol. Microbiol.* **102**, 183–195 (2016).
5. Liu, G., Chater, K. F., Chandra, G., Niu, G. & Tan, H. Molecular regulation of antibiotic biosynthesis in *Streptomyces*. *Microbiol. Mol. Biol. Rev.* **77**, 112–143 (2013).
6. Cho, J. S., Kim, G. B., Eun, H., Moon, C. W. & Lee, S. Y. Designing microbial cell factories for the production of chemicals. *JACS Au* **2**, 1781–1799 (2022).
7. Volk, M. J. et al. Metabolic engineering: methodologies and applications. *Chem. Rev.* **123**, 5521–5570 (2023).
8. Fang, L. et al. Genome-scale target identification in *Escherichia coli* for high-titer production of free fatty acids. *Nat. Commun.* **12**, 4976 (2021).
9. Yu, X. et al. CRISPRi-microfluidics screening enables genome-scale target identification for high-titer protein production and secretion. *Metab. Eng.* **75**, 192–204 (2023).
10. Esvelt, K. M. & Wang, H. H. Genome-scale engineering for systems and synthetic biology. *Mol. Syst. Biol.* **9**, 641 (2013).
11. Si, T., Xiao, H. & Zhao, H. Rapid prototyping of microbial cell factories via genome-scale engineering. *Biotechnol. Adv.* **33**, 1420–1432 (2015).
12. Hanna, R. E. & Doench, J. G. Design and analysis of CRISPR-Cas experiments. *Nat. Biotechnol.* **38**, 813–823 (2020).
13. Klann, T. S. et al. CRISPR-Cas9 epigenome editing enables high-throughput screening for functional regulatory elements in the human genome. *Nat. Biotechnol.* **35**, 561–568 (2017).
14. Schuster, A. et al. RNAi/CRISPR screens: from a pool to a valid hit. *Trends Biotechnol.* **37**, 38–55 (2019).

15. Sarnaik, A., Liu, A., Nielsen, D. & Varman, A. M. High-throughput screening for efficient microbial biotechnology. *Curr. Opin. Biotechnol.* **64**, 141–150 (2020).
16. Tucker, A. T. et al. Discovery of next-generation antimicrobials through bacterial self-screening of surface-displayed peptide libraries. *Cell* **172**, 618–628.e613 (2018).
17. Lee, S. W. & Oh, M. K. A synthetic suicide riboswitch for the high-throughput screening of metabolite production in *Saccharomyces cerevisiae*. *Metab. Eng.* **28**, 143–150 (2015).
18. Ruiz, B. et al. Production of microbial secondary metabolites: regulation by the carbon source. *Crit. Rev. Microbiol.* **36**, 146–167 (2010).
19. Mani, R. et al. Defining genetic interaction. *Proc. Natl Acad. Sci. USA* **105**, 3461–3466 (2008).
20. Boone, C., Bussey, H. & Andrews, B. J. Exploring genetic interactions and networks with yeast. *Nat. Rev. Genet.* **8**, 437–449 (2007).
21. Cao, J. Y. et al. Prognostic significance and therapeutic implications of centromere protein F expression in human nasopharyngeal carcinoma. *Mol. Cancer* **9**, 237 (2010).
22. Gaudelli, N. M., Long, D. H. & Townsend, C. A. β-Lactam formation by a non-ribosomal peptide synthetase during antibiotic biosynthesis. *Nature* **520**, 383–387 (2015).
23. Li, Z. et al. Stepwise increase of thaxtomins production in *Streptomyces albidoflavus* J1074 through combinatorial metabolic engineering. *Metab. Eng.* **68**, 187–198 (2021).
24. Koglin, A. et al. Structural basis for the selectivity of the external thioesterase of the surfactin synthetase. *Nature* **454**, 907–911 (2008).
25. Ng, I. S., Ye, C., Zhang, Z., Lu, Y. & Jing, K. Daptomycin antibiotic production processes in fed-batch fermentation by *Streptomyces roseosporus* NRRL11379 with precursor effect and medium optimization. *Bioprocess Biosyst. Eng.* **37**, 415–423 (2014).
26. Zhao, X., Zong, Y., Wei, W. & Lou, C. Multiplexed promoter engineering for improving thaxtomin A production in heterologous *Streptomyces* hosts. *Life* **12**, 689 (2022).
27. Wang, X. R. et al. Elucidation of genes enhancing natural product biosynthesis through co-evolution analysis. *Nat. Metab.* **6**, 933–946 (2024).
28. Kirby, R. Chromosome diversity and similarity within the Actinomycetales. *FEMS Microbiol. Lett.* **319**, 1–10 (2011).
29. Yan, H., Li, S. & Wang, W. Reprogramming naturally evolved switches for *Streptomyces* chassis development. *Trends Biotechnol.* **43**, 12–15 (2024).
30. Yan, H. et al. BldD, a master developmental repressor, activates antibiotic production in two *Streptomyces* species. *Mol. Microbiol.* **113**, 123–142 (2020).
31. Mao, X. M. et al. Transcriptional regulation of the daptomycin gene cluster in *Streptomyces roseosporus* by an autoregulator. *AtrA. J. Biol. Chem.* **290**, 7992–8001 (2015).
32. Chen, Q., Zhu, J., Li, X. & Wen, Y. Transcriptional regulator DasR represses daptomycin production through both direct and cascade mechanisms in *Streptomyces roseosporus*. *Antibiotics* **11**, 1065 (2022).
33. Huang, X. et al. *wblA*, a pleiotropic regulatory gene modulating morphogenesis and daptomycin production in *Streptomyces roseosporus*. *J. Appl. Microbiol.* **123**, 669–677 (2017).
34. Tong, Y. et al. CRISPR-Cas9, CRISPRi and CRISPR-BEST-mediated genetic manipulation in streptomycetes. *Nat. Protoc.* **15**, 2470–2502 (2020).
35. Jin, Z. J. About the evaluation of drug combination. *Acta Pharmacol. Sin.* **25**, 146–147 (2004).
36. Pérez-Pérez, J. M., Candela, H. & Micol, J. L. Understanding synergy in genetic interactions. *Trends Genet.* **25**, 368–376 (2009).
37. Cai, P. et al. Recombination machinery engineering facilitates metabolic engineering of the industrial yeast *Pichia pastoris*. *Nucleic Acids Res.* **49**, 7791–7805 (2021).
38. Adrio, J. L. & Demain, A. L. Genetic improvement of processes yielding microbial products. *FEMS Microbiol. Rev.* **30**, 187–214 (2006).
39. Barreiro, C. & Garcia-Estrada, C. Proteomics and *Penicillium chrysogenum*: Unveiling the secrets behind penicillin production. *J. Proteom.* **198**, 119–131 (2019).
40. Zeng, W., Guo, L., Xu, S., Chen, J. & Zhou, J. High-throughput screening technology in industrial biotechnology. *Trends Biotechnol.* **38**, 888–906 (2020).
41. Han, K. et al. Synergistic drug combinations for cancer identified in a CRISPR screen for pairwise genetic interactions. *Nat. Biotechnol.* **35**, 463–474 (2017).
42. Mao, X. M., Luo, S. & Li, Y. Q. Negative regulation of daptomycin production by DepR2, an ArsR-family transcriptional factor. *J. Ind. Microbiol. Biotechnol.* **44**, 1653–1658 (2017).
43. Luo, S., Chen, X. A., Mao, X. M. & Li, Y. Q. Transposon-based identification of a negative regulator for the antibiotic hyperproduction in *Streptomyces*. *Appl. Microbiol. Biotechnol.* **102**, 6581–6592 (2018).
44. Sastry, A. V. et al. The *Escherichia coli* transcriptome mostly consists of independently regulated modules. *Nat. Commun.* **10**, 5536 (2019).
45. Askenazi, M. et al. Integrating transcriptional and metabolite profiles to direct the engineering of lovastatin-producing fungal strains. *Nat. Biotechnol.* **21**, 150–156 (2003).
46. Xiang, S. H. et al. Application of a double-reporter-guided mutant selection method to improve clavulanic acid production in *Streptomyces clavuligerus*. *Metab. Eng.* **11**, 310–318 (2009).
47. Wang, J. Y. & Doudna, J. A. CRISPR technology: A decade of genome editing is only the beginning. *Science* **379**, 251 (2023).
48. Li, X., Sang, Z., Zhao, X. & Wen, Y. Metabolic engineering of *Streptomyces roseosporus* for increased production of clinically important antibiotic daptomycin. *Microb. Biotechnol.* **17**, e70038 (2024).
49. Zhang, Q. et al. A MarR family transcriptional regulator, DptR3, activates daptomycin biosynthesis and morphological differentiation in *Streptomyces roseosporus*. *Appl. Environ. Microbiol.* **81**, 3753–3765 (2015).
50. Gomez-Escribano, J. P. & Bibb, M. J. Engineering *Streptomyces coelicolor* for heterologous expression of secondary metabolite gene clusters. *Microb. Biotechnol.* **4**, 207–215 (2011).
51. Li, P. et al. An efficient blue-white screening based gene inactivation system for *Streptomyces*. *Appl. Microbiol. Biotechnol.* **99**, 1923–1933 (2015).
52. Bierman, M. et al. Plasmid cloning vectors for the conjugal transfer of DNA from *Escherichia coli* to *Streptomyces* spp. *Gene* **116**, 43–49 (1992).
53. Tong, Y. et al. Highly efficient DSB-free base editing for streptomycetes with CRISPR-BEST. *Proc. Natl Acad. Sci. USA* **116**, 20366–20375 (2019).
54. Li, L. et al. CRISPR-Cpf1-assisted multiplex genome editing and transcriptional repression in *Streptomyces*. *Appl. Environ. Microbiol.* **84**, e00827–18 (2018).
55. Smith, K. & Youngman, P. Use of a new integrational vector to investigate compartment-specific expression of the *Bacillus subtilis spoIIM* gene. *Biochimie* **74**, 705–711 (1992).
56. Spizizen, J. Transformation of biochemically deficient strains of *Bacillus subtilis* by deoxyribonucleate. *Proc. Natl Acad. Sci. USA* **44**, 1072–1078 (1958).
57. Wu, Q., Zhi, Y. & Xu, Y. Systematically engineering the biosynthesis of a green biosurfactant surfactin by *Bacillus subtilis* 168. *Metab. Eng.* **52**, 87–97 (2019).
58. Miller, G. L. Use of dinitrosalicylic acid reagent for determination of reducing sugar. *Anal. Chem.* **31**, 426–428 (1959).
59. Zhao, Y. et al. CRISPR/dCas9-mediated multiplex gene repression in *Streptomyces*. *Biotechnol. J.* **13**, e1800121 (2018).
60. Wu, Y. et al. CAMERS-B: CRISPR/Cpf1 assisted multiple-genes editing and regulation system for *Bacillus subtilis*. *Biotechnol. Bioeng.* **117**, 1817–1825 (2020).

Acknowledgements
This study was supported by the National Natural Science Foundation of China (Grant No. 32170081 to Y.W., 32100066 to H.Y., and 32170095 to W.W.) and the National Key Research and Development Program of China (Grant No. 2021YFC2100602 to W.W.).

Author contributions
W.W., Y.W., and H.Y. designed the research. H.Y. conducted most of the experiments. Z.S., Z.X., X.L., J.X., J.W. and S.P. conducted part of the experiments. W.W., W.W., and H.Y. contributed reagents/materials/analysis tools. W.W., Y.W., and H.Y. wrote the paper with contributions from all other authors.

Competing interests
W.W., Y.W., H.Y., Z.X. and Z.S. have filed provisional patents for this work to the China National Intellectual Property Administration (CNIPA). The patent application numbers are CN202210143368.8, CN202410571683.X, CN202510175729.0 and CN202510175726.7. The remaining authors declare no competing interests.

Additional information
Supplementary information The online version contains supplementary material available at https://doi.org/10.1038/s41467-025-57073-5.

Correspondence and requests for materials should be addressed to Ying Wen or Weishan Wang.

Peer review information *Nature Communications* thanks the anonymous reviewers for their contribution to the peer review of this work. A peer review file is available.